Science of the Total Environment 648 (2019) 481–499

Contents lists available at ScienceDirect

Science of the Total Environment

journal homepage: www.elsevier.com/locate/scitotenv

Assessing the impacts of future climate change on the hydroclimatology of the Gediz Basin in Turkey by using dynamically downscaled CMIP5 projections

Merve Gorguner [a,*], M. Levent Kavvas [a], Kei Ishida [b]

[a] Department of Civil and Environmental Engineering, University of California, Davis, CA 95616, USA
[b] Department of Civil and Environmental Engineering, Kumamoto University, Kumamoto 860-8555, Japan

HIGHLIGHTS

- Dynamical downscaling of eight CMIP5 future climate projections
- Coupling of a regional climate model and a physically-based hydrology model
- Increasing trend in average annual temperature of the ensemble of all projections
- Decreasing trend in average annual inflows of the ensemble of all projections

GRAPHICAL ABSTRACT

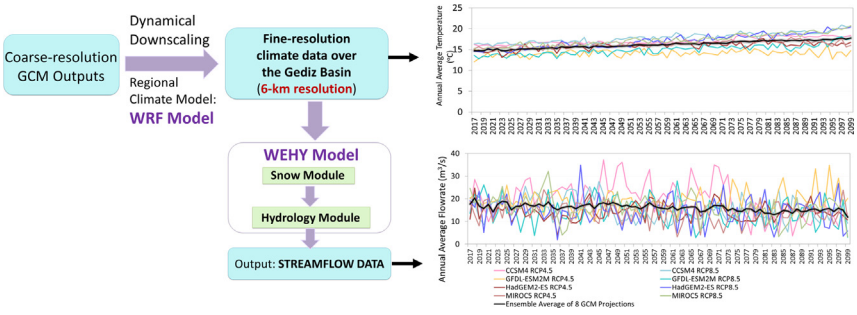

ARTICLE INFO

Article history:
Received 26 May 2018
Received in revised form 11 August 2018
Accepted 12 August 2018
Available online 13 August 2018

Editor: D. Barcelo

Keywords:
GCM
Mediterranean
Regional climate model
Water resources
WEHY model
WRF model

ABSTRACT

The Gediz Basin is a Mediterranean watershed along the Aegean coast of Turkey, in which the most important economic activity is agriculture. Over the last few decades, this basin has been experiencing water-related problems such as water scarcity and competing use of water. This study assesses the impact of future climate change on the availability of water resources in the Gediz Basin during the 21st century by investigating the inflows into the major reservoir in the basin, Demirkopru Reservoir, which is the major source of irrigation water to the basin. The analysis in this study involves setting up a coupled hydro-climate model over the Gediz Basin by coupling the Weather Research and Forecasting (WRF) model to the physically-based Watershed Environmental Hydrology (WEHY) model. First, the WRF model is used to reconstruct the historical climatic variables over the basin by dynamically downscaling the ERA-Interim reanalysis dataset. The calibrated and validated WRF model is then used to dynamically downscale eight different future climate projections over the Gediz Basin to a much finer resolution (6 km), which is more appropriate for the hydrologic modeling of the basin. These climate projections are from four Coupled Model Intercomparison Project Phase 5 (CMIP5) Global Climate Models (GCMs), namely, CCSM4, GFDL-ESM2M, HadGEM2-ES, and MIROC5, under two IPCC (The Intergovernmental Panel on Climate Change) representative concentration pathway scenarios (RCP4.5 and RCP8.5). The outputs from the WRF model are then input into the WEHY model, which is calibrated and validated over the basin, to simulate the hydrological processes within the basin and to obtain the projected future inflows into the Demirkopru Reservoir. Results of the future analysis over the 21st century (2017–2100) are then compared to the historical values (1985–2012) to investigate the impacts of future climate change on the hydroclimatology of the Gediz Basin.

* Corresponding author.
E-mail addresses: gorguner@ucdavis.edu (M. Gorguner), mlkavvas@ucdavis.edu (M.L. Kavvas), keiishida@kumamoto-u.ac.jp (K. Ishida).

https://doi.org/10.1016/j.scitotenv.2018.08.167
0048-9697/

1. Introduction

As much as the current climate is important to today's human activities, its future projections play an important role in alerting scientists and policy-makers to the expected impacts of future climate change. With such projections, the appropriate mitigation or adaptive measures can be accordingly planned for. Under a changing climate, increasing atmospheric concentrations of carbon dioxide and other trace gases released to the atmosphere due to a number of natural and anthropogenic processes bring about climatic alterations that have substantial impacts on the global hydrological system and water resources (Piao et al., 2007; Gerten et al., 2008). Moreover, the timing and magnitude of surface runoff and soil moisture, as well as the water availability are affected by these changes in the climate system (Gleick, 1989; Kundzewicz et al., 2008; Hidalgo et al., 2009). For this reason, hydrological impact analysis of future climate change has become a thriving area of research.

Over the last few decades, numerous studies have been carried out to investigate future climate change impacts on river flows and water resources at global (Arnell, 1999a, 2003; van Vliet et al., 2013), continental (Arnell, 1999b; Lehner et al., 2006), and regional scales (Nohara et al., 2006; Li et al., 2013; Bohner et al., 2014; Smiatek et al., 2014; Amin et al., 2017). Such studies are usually based on the climate projections of Global Climate Models (GCMs), which are also known as General Circulation Models. GCMs are the most powerful tools available today to understand the global climate system, and to project future climate change, which is associated with a variety of anthropogenic greenhouse gas emission scenarios (McGuffie and Henderson-Sellers, 2001). The capability of the GCMs in terms of how well they represent the physical climatic processes and reproduce the observed phenomena greatly affects the reliability of the projected changes in climate (ul Hasson et al., 2016). Several such GCMs were used by climate modeling groups from around the world to support the development of the Intergovernmental Panel on Climate Change (IPCC)'s Fifth Assessment Report (AR5) through a set of climate model experiments, known as the Coupled Model Intercomparison Project Phase 5 (CMIP5) (Taylor et al., 2012). CMIP5 experiments were designed to enhance the understanding of the climate, and to help simulate the possible effects of future climate change under the scenarios known as the Representative Concentration Pathways (RCPs) (Moss et al., 2010). The RCPs focus on the 'concentrations' of greenhouse gas emissions, which will cause climate change, and they include 'pathways' that these concentrations will follow over time to reach a particular radiative forcing by the year 2100. Radiative forcing levels for the set of four RCPs, adopted by the IPCC, are 2.6, 4.5, 6.0 and 8.5 W/m^2 by the end of the 21st century for RCP2.6, RCP4.5, RCP6.0 and RCP8.5, respectively (van Vuuren et al., 2011).

However, due to the GCMs' coarse spatial resolutions, which generally exceed 100 km, the GCMs are not able to account for the effect of regional- and watershed-scale land conditions on the climate, and thus they are not able to resolve cloud formation, soil moisture transfer or the mesoscale processes such as convection and orographic effects (McGuffie and Henderson-Sellers, 2001; Christensen and Christensen, 2003; Fowler et al., 2007; Jang et al., 2017). To overcome the scale incompatibility problem between the coarse-resolution GCM outputs (or reanalysis data) and the resolution required for regional- or watershed-scale impact assessment, a downscaling technique is required (Maraun et al., 2010). There are two fundamental downscaling techniques: (1) statistical downscaling, which is done by relating GCM-resolution climate variables and local observation data empirically with a statistical relationship (Wilby and Wigley, 1997; Wilby et al., 1998), and (2) dynamical downscaling, in which a fine-resolution regional climate model (RCM) is embedded within a GCM to obtain local weather variables by the explicit solution of the process-based physical dynamics of the system (Xu, 1999; Fowler et al., 2007; Spak et al., 2007). Both downscaling techniques have advantages and disadvantages, and their outputs could change based on the study area and various spatial and temporal scales (Jang and Kavvas, 2015). Although statistical downscaling requires less computational effort and is easier to apply than dynamical downscaling, it depends on the fundamental assumption of climate stationarity and it cannot incorporate the natural variability of the climate system (Fowler et al., 2007; Jang and Kavvas, 2015). Dynamical downscaling, on the other hand, is not restricted to such stationarity assumptions because it uses the same fundamental equations as a GCM to represent atmospheric dynamical and physical processes. As a result, dynamical downscaling has the advantage of being a physically based method that conserves the mass, momentum, and energy in the system, and that incorporates all topographical and natural factors into its downscaled atmospheric variables.

The downscaled atmospheric variables from GCMs are usually used as inputs into watershed hydrology models, thus making it possible to assess the impacts of climate change on a regional scale. These watershed hydrology models are used to represent the dynamic interactions occurring between the climate and the land surface hydrology. For instance, vegetation, snow cover, and permafrost active layer are all very susceptible to the changes in the lower boundary layer of the atmosphere. The hydrologic characteristics are affected significantly by the moisture and heat transfer between the land surface and atmosphere, which yield the lower boundary conditions for the climate modeling (Kavvas et al., 1998). Hence, using hydrologic models to assess the impacts of climate change has many attractive characteristics. First, the models are readily available to simulate various climatic conditions, and some are even established to run for different dominant hydrologic process representations and spatial scales. This provides flexibility in defining and selecting the most appropriate model for the evaluation of any particular watershed/region. Second, hydrologic models can be adjusted to run the characteristics of the available data. Since GCM-derived climate change scenarios, which are obtained from different levels of downscaling, can be used as hydrologic model inputs, a variety of hydrological responses to climate change scenarios can be simulated. Third, hydrologic models are relatively easier to tailor than GCMs. Fourth, hydrologic models can be used to assess the sensitivity of particular watersheds to climate change scenarios obtained from GCMs (Gleick, 1989; Schulze, 1997).

It is important to note, however, that uncertainties in the future simulations of both the hydrologic and climate models still exist, in spite of the improvements in their respective performances. The most significant source of uncertainty comes from the GCMs used (Wilby et al., 2006; Graham et al., 2007). Since different GCMs simulate atmospheric conditions and feedbacks by using different parameterizations and schemes, they differ widely in their projections, especially for precipitation (Wilby and Harris, 2006). Greenhouse gas emission scenarios, the conversion of emissions into atmospheric concentrations, and the associated radiative forcings also contribute to the uncertainty arising from GCM simulations (New and Hulme, 2000; Allen et al., 2001; Webster et al., 2003). Another source of uncertainty is the downscaling techniques, and this is due to the assumptions that are inherent in these techniques. As more assumptions are made with each modeling stage, uncertainties are naturally added to the computations (Trzaska and Schnarr, 2014). A third source of uncertainty arises from the selection of the hydrologic model. This is because hydrologic models use different sets of parameters and assumptions to simulate runoff at particular spatial and temporal scales (Praskievicz and Chang, 2009). Therefore, with all these uncertainties influencing the results of future simulations, an effective way to increase the reliability of long-term future projections would be through the use of an ensemble of model simulations. This is because predictions of climatic response to external forcings could be based on the statistical properties of these ensembles of simulations (Giorgi and Francisco, 2000; Raisanen and Palmer, 2001; Tebaldi and Knutti, 2007). Such an ensemble of simulations can be obtained by performing the required simulations for several of the GCM climate projections, thus providing the results for all these projections which would in turn help in understanding the expected future behavior through the study of their statistical properties.

The goal of this study is to assess the impacts of climate change on the hydroclimatology of a Mediterranean basin known as the Gediz Basin, which is an agriculture-dominant basin in Western Turkey. The Gediz Basin was historically a water-rich basin, but over the last few decades, the availability of water in the Gediz Basin has decreased substantially. The status of the basin is now classified as a closed basin, in which there is no unused water left to be allocated (Svendsen et al., 2005). The primary problem currently in the Gediz Basin is that the consumption of water is more than what is sustainable, which leads to water scarcity and to conflicts among water users. Hence, it is important to assess possible future changes in water availability of this basin under changing climate to implement better water resources management strategies. To accomplish this, this research mainly focuses on the Demirkopru Reservoir, which is the major reservoir in the basin that provides irrigation water to an extensive irrigation system, and it investigates the future inflows into the reservoir under a changing climate during the 21st century. An integrated approach to climate change impact assessment is explored by coupling an atmospheric model and a hydrologic model within a hydro-climate modeling framework. Kelley et al. (2012) showed that the hydrological cycle in the Mediterranean is represented better both spatially and seasonally using CMIP5 models compared to CMIP3 (the climate model experiments that contributed to the IPCC's Fourth Assessment Report) models, possibly because CMIP5 models were run at finer resolutions. Hence, four GCM outputs selected from the CMIP5 archive under two different representative concentration pathway scenarios (RCP4.5 and RCP8.5) were dynamically downscaled over the Gediz Basin to simulate the future hydro-climatic conditions for the years 2017 to 2100. The resultant fine-resolution global atmospheric data were then used to drive a spatially distributed snowmelt model to simulate (temporally and spatially) the amount of precipitation water kept in the snowpack and the released water from the snowpack. Then, a fully physically-based distributed hydrologic model with the capability of interaction between atmospheric and hydrologic processes was used to simulate the hydrologic processes over the Gediz Basin under climate change during the 21st century, from which the projected future inflows into the Demirkopru Reservoir were obtained and analyzed.

2. Materials and methods

2.1. Study area

The Gediz Basin is a watershed along the Aegean coast of Turkey with a catchment area of 17,000 km^2. A topographical map of the basin showing the boundaries of the catchment area, the major river system with its main tributaries, meteorological stations, stream gauging stations, and reservoirs is given in Fig. 1. The basin lies between the northern latitudes of 38°04′ N and 39°13′ N and the eastern longitudes of 26°42′ E and 29°45′ E. It is bounded on the north, east and south by high mountains, and on the west by the Aegean Sea. The highest altitude inside the basin is around 2300 m above mean sea level. The natural vegetation of the basin is mainly bush and forest. The major river of the Gediz Basin, the Gediz River, is borne inside the basin and flows into the Gulf of Izmir (Aegean Sea) after being fed by many tributaries.

The Gediz Basin began to form during the Quaternary period (Hakyemez et al., 2013). It includes Menderes Massif, a major polymetamorphic complex in Western Turkey (Biricik, 1995; Koralay, 2015). The erosional activities of the Gediz River caused a portion of this massif to erode and disintegrate from its upper layer. The alluvium transported by the Gediz River formed the productive plains in the basin, which settled in the grabens formed by epeirogenic tectonic movements. The water infiltrated through the soil column is known to be stored in the Quaternary deposits, and forms the aquifers and even the artesian basins in some places (Biricik, 1995; Hakyemez et al., 2013).

The Gediz Basin has a typical Mediterranean climate. The movement of frontal cyclones towards continental interiors, which occurs due to the deep valleys elongated from west to east, brings about precipitation along those valleys. The basin is influenced by the north-westerly upper air flows and frontal Mediterranean cyclones related to the south-westerly air flows, which result in heavy rainfalls in late-autumn, winter and spring. Furthermore, convective storms and some frontal thunderstorms cause precipitation over the continental interiors in spring and early summer. The topography and exposure can cause microclimatic variations in the basin, and hence affect the mesoscale weather systems in all seasons (Turkes, 1996).

The historical mean annual temperature and the historical mean annual precipitation of the Gediz Basin are 15.6 °C and 635 mm, respectively. The basin receives precipitation between November and April, where 75% of the total annual precipitation is recorded between November and March. As such, the wettest months are January and February, and the driest months are July and August. Higher inland areas receive an annual precipitation of around 800 mm, whereas this value decreases to 450 mm near the coast. As for the stream discharge, the Gediz River has a mean annual flow of 46 m^3/s (Droogers et al., 2000), and peak flows are usually observed in the months of February or March. Under natural conditions, when many of the small tributaries of the streams dry up, stream discharge decreases from the winter months up until May (Ulke et al., 2009; Yilmaz and Harmancioglu, 2012). In summer, only the Gediz River and its large tributaries have

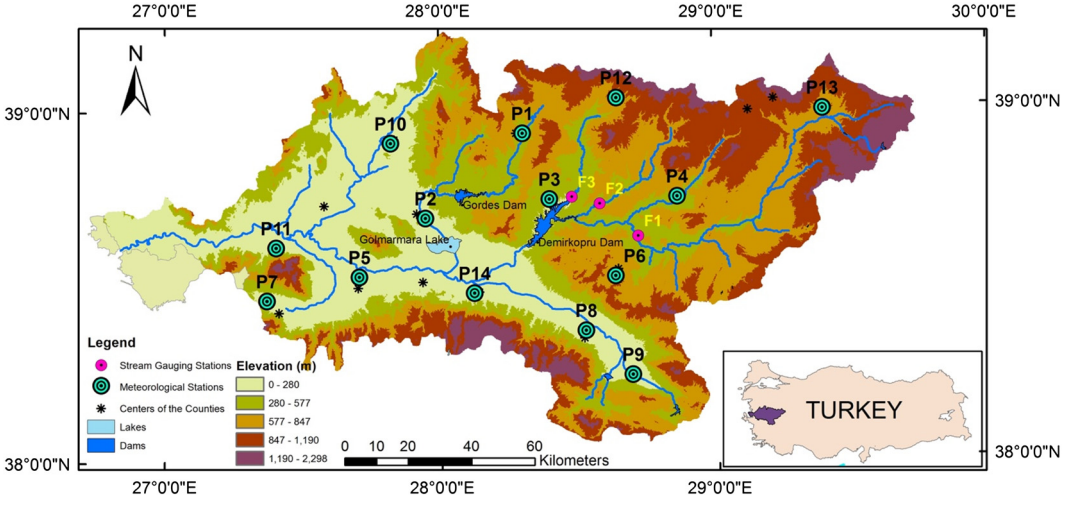

Fig. 1. Geographic location and elevation map of the Gediz Basin, along with the locations of meteorological and stream gauging stations.

flows, and even these flows may be negligible during the warmest months. After the irrigation season, the only flows that occur in the basin are from the few larger tributaries, which include the residual return flows from irrigated fields, and discharges of industrial and municipal wastewater treatment plants into the river (Svendsen et al., 2005).

It is significant to note that the most important economic activity in the Gediz Basin is agriculture. An area with a size of approximately 110,000 ha (1100 km^2) is subject to extensive agricultural activities with a large irrigation system (Gediz irrigation system). Similar to other agriculture-dominant basins, the most significant use of surface water in the Gediz Basin is for irrigation, which uses about 75% of all fresh surface water available in the basin (Yilmaz and Harmancioglu, 2010). The Gediz Basin also has three major reservoirs: the Demirkopru Dam, the Golmarmara Lake, and the Gordes Reservoir. Demirkopru Dam, which is the largest and major dam in the Gediz Basin, was built between the years 1954 and 1960 to provide water for irrigation, to control floods, and to generate hydropower (i.e., 69 MW-capacity). The reservoir has an active storage volume of 1022 million m^3 (DSI, 2015). The amount of water stored in the Demirkopru Dam determines the volume and duration of irrigation water supplied to the Gediz irrigation system. The Gordes Reservoir, on the other hand, is much more recent, and was built between 1998 and 2012 (DSI, 2015). According to the National News (Bolulu, 2015; Sen, 2015), the Gordes Reservoir went under maintenance in 2015 due to a structural problem that had existed since the dam was built. For this reason, no data regarding the operation or inflow of this dam is available. There is also a lack of data regarding the operation of the regulated natural lake Lake Golmarmara, which serves as an extra source of water when the irrigation is intense during summer months. As such, the Demirkopru Dam is the only water system in the Gediz Basin with available data.

2.2. Data and model implementation

This study utilizes a coupled hydroclimate model, called Watershed Environmental Hydrology Hydro-Climate Model (WEHY-HCM), to assess the hydroclimatology of the Gediz Basin under future climate projections within a hydro-climate modeling framework. The WEHY-HCM is comprised of an atmospheric model component and a watershed hydrology model component. The methodology followed in this paper is presented in Fig. 2. After the atmospheric model is used to dynamically downscale the reanalysis or climate projection data into finer resolutions, the outputs of this model are input into the snow model to simulate the snow accumulation and melting processes. The snow model outputs are then used as inputs into the hydrology model, which will in turn simulate the formation of the hydrologic processes within the Gediz Basin, both temporally and spatially, to obtain the streamflows within the basin for the historical period and for the future climate projections. From these results, the historical and future inflows into the Demirkopru Reservoir can be obtained. As such, through the implementation of the WEHY-HCM over the Gediz Basin, it is possible to assess the hydroclimatology of the basin under future climate change projections, and it is possible to compare the historical basin hydroclimate conditions and Demirkopru reservoir inflows to their corresponding future projections.

2.2.1. Atmospheric model component setup

The WEHY-HCM employs an RCM as its atmospheric model component. In this study, the Weather Research and Forecasting (WRF) model (Skamarock et al., 2008) was selected as the RCM for the WEHY-HCM. The WRF model is a fully compressible and non-hydrostatic model, which is a successor of NCAR/Penn State University meteorological model MM5. It is used in many applications such as, data assimilation and forecast research, regional climate studies and coupled-model applications. Real data (observations, analyses) or idealized conditions of the atmosphere that have scales from meters to thousands of kilometers can be simulated by the model (WRF-ARW, 2015). The data and the methodology used to set up the WRF model over the Gediz Basin are described below.

2.2.1.1. Station observation data. Observed daily average temperature and daily total precipitation data were obtained from the Turkish State Meteorological Service (DMI). The locations of the 14 meteorological

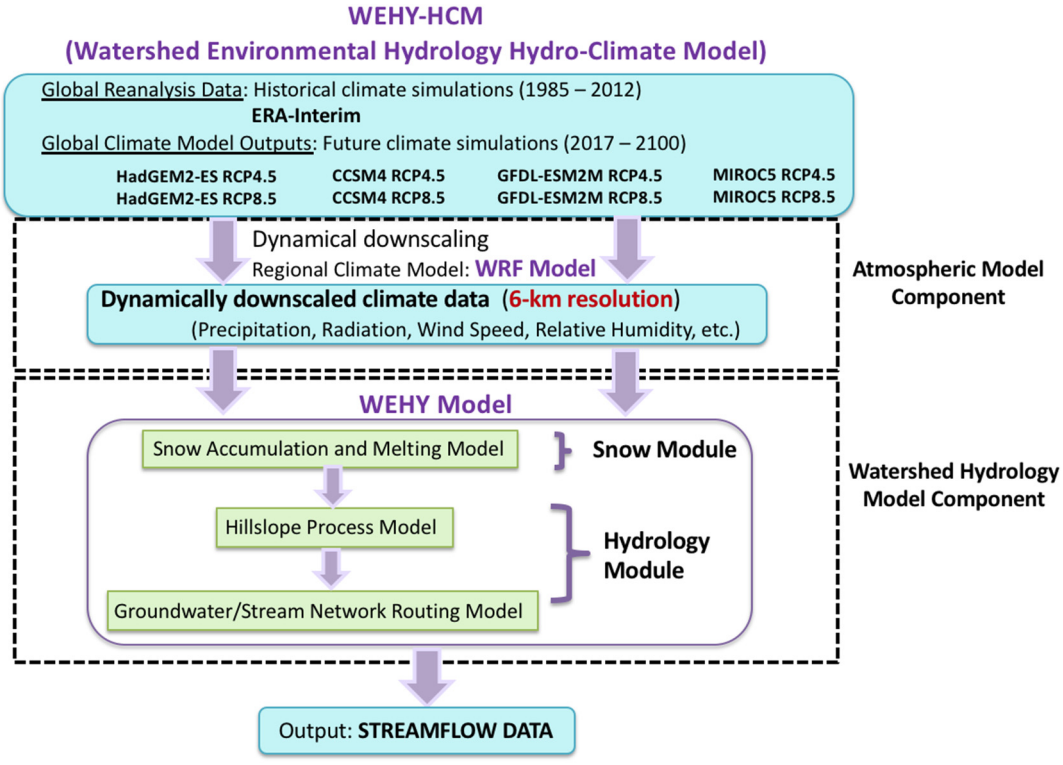

Fig. 2. Model components of the WEHY-HCM.

Table 1
Details of the meteorological stations in the Gediz Basin used in this study.

#	Station number	Station name	Latitude	Longitude	Altitude (MSL)	Measurement period
P1	4930	Gordes	38.9366° N	28.3038° E	622 m	1981–1996
P2	5273	Golmarmara	38.6972° N	27.9481° E	92 m	1984–1991
P3	5278	Koprubasi	38.7482° N	28.3992° E	250 m	1987–2006
P4	5282	Selendi	38.7511° N	28.8639° E	475 m	1986–1990
P5	5615	Turgutlu	38.5312° N	27.7065° E	45 m	1984–2006
P6	5624	Kula	38.5272° N	28.6368° E	720 m	1986–1989
P7	5785	Kemalpasa	38.4639° N	27.3705° E	208 m	1970–1997
P8	5974	Alasehir	38.3730° N	28.5266° E	189 m	1970–2006
P9	6143	Sarigol	38.2453° N	28.6939° E	203 m	1984–1986
P10	17184	Akhisar	38.9118° N	27.8233° E	92 m	1970–2014
P11	17186	Manisa	38.6153° N	27.4049° E	71 m	1970–2014
P12	17746	Demirci	39.0349° N	28.6482° E	855 m	1992–2011
P13	17750	Gediz	38.9947° N	29.4003° E	736 m	1972–2011
P14	17792	Salihli	38.4831° N	28.1234° E	111 m	1970–2011

stations within the Gediz Basin, whose temperature and precipitation data were used in this study, are shown in Fig. 1. Although their record lengths vary, data from all the stations that were available from 1970 to 2014 were obtained. The coordinates, altitudes above mean sea level, and measurement periods of these stations are listed in Table 1.

2.2.1.2. Reanalysis data. In addition to the observed data, the global historical reanalysis dataset ERA-Interim for the years 1984 to 2013 was obtained. ERA-Interim is the most recent global atmospheric reanalysis produced by the European Centre for Medium-Range Weather Forecasts (ECMWF), and has a horizontal resolution of approximately 80 km (Dee et al., 2011). Global reanalysis datasets have been used in downscaling studies to reconstruct the historical atmospheric data especially in regions where monitoring network is sparse or even nonexistent (Ohara et al., 2011; Kavvas et al., 2013; Kure et al., 2013; Ishida et al., 2017).

2.2.1.3. CMIP5 data. To study the climate change impacts on the future hydroclimatology of the Gediz Basin, the projections of four different CMIP5 GCMs running under two RCP scenarios were obtained and used in this study. The selected GCMs (HadGEM2-ES, GFDL-ESM2M, MIROC5 and CCSM4) were developed by four different climate research groups. Details of the four GCMs applied in this study are listed in Table 2. The two RCP climate scenarios selected were RCP4.5 and RCP8.5. RCP4.5 is an intermediate stabilization emission scenario with 'strong mitigation' whose total radiative forcing is stabilized before 2100 and reaches to 4.5 W/m^2 by 2100 (~650 ppm CO_2 equivalent). It assumes that emissions are being restricted globally due to prices imposed on the emissions coupled with simultaneous emissions mitigation strategies. Further details about this pathway can be found in Smith and Wigley (2006), Clarke et al. (2007), and Wise et al. (2009). On the other hand, RCP8.5 is an emission scenario with very high baseline emission, whose radiative forcing leads to 8.5 W/m^2 by 2100 (equivalent to 1370 ppm CO_2 equivalent). RCP8.5 is also known as the 'baseline' scenario that does not include any specific climate mitigation target (Riahi et al., 2011).

2.2.1.4. WRF model setup and experimental design. With the required atmospheric data having been obtained, it was possible to set up the WRF model over the Gediz Basin. The climate variables produced by the WRF model included precipitation, surface pressure, wind speed, geopotential height, downward longwave and shortwave radiation, and air temperature. The WRF model was initially used to reconstruct the historical atmospheric data over the Gediz Basin, between 1985 and 2012, by dynamically downscaling the ERA-Interim reanalysis data. This downscaling procedure was done by configuring the WRF model with three nested domains, as shown in Fig. 3, with grid resolutions of 54 km × 54 km, 18 km × 18 km, and 6 km × 6 km. The coarse outer domain, named D01, comprised the southeast Europe, Black Sea, a part of Turkey, the Aegean Sea and the eastern Mediterranean Sea. The second domain, named D02, covered the western half of Turkey and the Aegean Sea. The third domain, named D03, comprised the entire Gediz Basin, with the Gediz Basin located in the center. D01 consisted of 35 × 38 horizontal grids, D02 had 43 × 46 horizontal grids, and D03 had 55 × 43 horizontal grid points for the meridional and zonal directions, respectively. The initial and boundary condition atmospheric datasets for the historical period were taken from the ERA-Interim reanalysis data. As such, the WRF model could downscale the reanalysis data from their coarse resolutions to much finer resolutions, namely to a 6 km horizontal resolution with hourly temporal resolution over the Gediz Basin.

Before reconstructing the historical atmospheric data over the whole historical period, the WRF model was first calibrated for the water year 2006 by comparing its results to the observed total monthly precipitation data, which were recorded by seven meteorological stations that were in operation during the calibration year. Many different combinations of the parameterizations of the WRF model were tested until the best combination of WRF physics options was found. In this study, the selected physics schemes were the WRF Single-Moment 3-class (WSM3) microphysics scheme (Hong et al., 2004), the Tiedtke cumulus parameterization scheme (Tiedtke, 1989; Zhang et al., 2011), the Yonsei University planetary boundary layer scheme (Hong et al., 2006), and the rapid update cycle (RUC) land surface model (Smirnova et al., 1997, 2000).

Table 2
Four global climate models used for the analyses applied in this study.

Model name	Institution (country)	Spatial resolution (Long. × Lat.)	Reference
CCSM4	National Center for Atmospheric Research (United States)	0.90° × 1.25°	Gent et al. (2011)
GFDL-ESM2M	Geophysical Fluid Dynamics Laboratory (United States)	2.5° × 2.0°	Dunne et al. (2012), (2013)
HadGEM2-ES	Met Office Hadley Centre (United Kingdom)	1.875° × 1.250°	Jones et al. (2011)
MIROC5	The University of Tokyo Center for Climate System Research, National Institute for Environmental Studies, Japan, Japan Agency for Marine-Earth Science and Technology Frontier Research Center for Global Change (Japan)	1.4° × 1.4°	Watanabe et al. (2010)

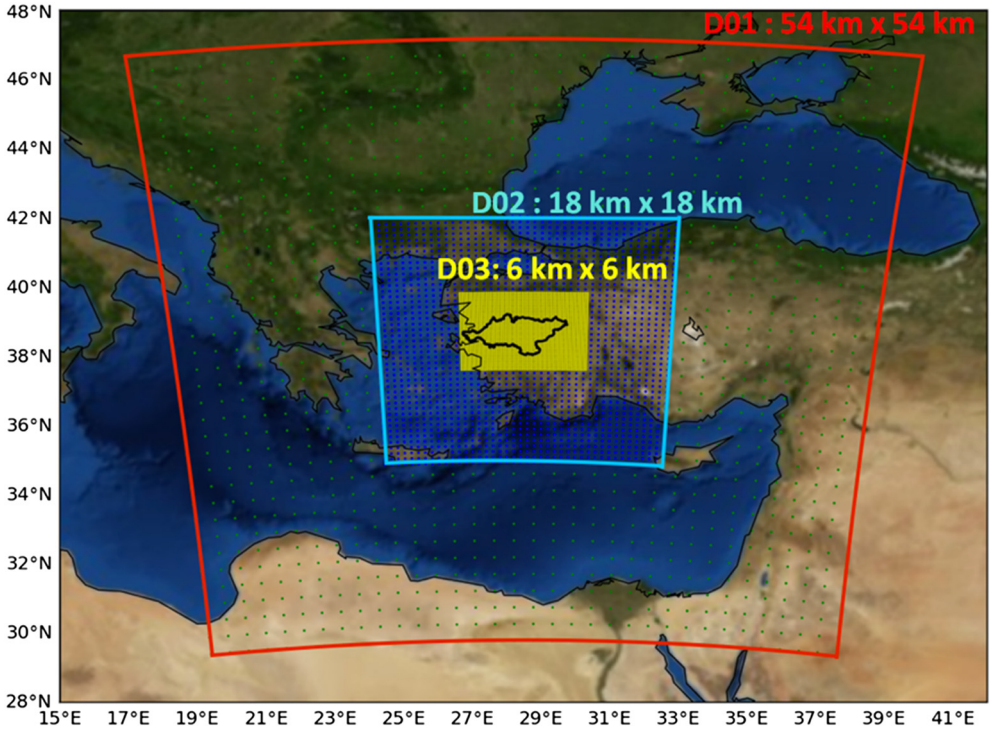

Fig. 3. The WRF model nested domain configuration over the Gediz Basin.

Following its calibration, the WRF model was validated for the water years from 1985 through 2012 by comparing the total monthly precipitation to the observed values of all the meteorological stations, as shown in Fig. 4. A statistical summary of the validation results for all stations is also listed in Table 3. In this study, the Nash-Sutcliffe model efficiency coefficient (NSE) and Pearson's correlation coefficient (R) were employed as the statistical parameters to assess the predictive capability of the model in simulating precipitation. As given in Table 3, the NSE coefficients varied between 0.54 and 0.83, and the R coefficients varied between 0.59 and 0.92. This indicated that the accuracy of the model simulations in representing the real historical climate was satisfactory. After the model validation was completed, the WRF model was also used to dynamically downscale the climate model projection outputs of HadGEM2-ES, MIROC5, CCSM4 and GFDL-ESM2M GCMs under RCP4.5 and RCP8.5 climate change scenarios. As such, the climatic variables of these future projections were downscaled from their coarse resolutions, ranging between 100 and 278 km, to a much finer resolution of 6 km in order to obtain the projected, fine resolution future atmospheric conditions over the Gediz Basin at 6 km grid resolution for the period 2017–2100.

2.2.2. Watershed hydrology model component setup

The watershed hydrology model component of the WEHY-HCM was selected in this study to be the Watershed Environmental Hydrology (WEHY) model. The WEHY model was developed by Kavvas et al. (2004) as a tool that uses upscaled hydrologic conservation equations through their ensemble-averaged forms and analyzes the formation of hydrologic processes within a watershed temporally and spatially by taking the heterogeneity of the watershed into account. The WEHY Model is a physically-based model using the conservation of mass, momentum, and/or energy equations of water flow in surface and subsurface flow domains of a watershed. It includes both a snow module and a hydrology module. Hence, the watershed hydrology model component of this study included the use of two modules of WEHY-HCM model, namely, Snow Module, and Hydrology Module, whose set up will be detailed below.

2.2.2.1. The WEHY-HCM Snow Module. The WEHY-HCM Snow Module, a spatially distributed snowmelt model, is an important component of the WEHY model used to evaluate the hydrologic regime in mountainous areas in a watershed. It models the amount of precipitation water kept in the snowpack and the released water from the snowpack in time. The WEHY-HCM Snow Module takes inputs including precipitation, surface pressure, wind speed, geopotential height, downward longwave and shortwave radiation, and air temperature, which are all common outputs from RCMs. In the WEHY-HCM Snow Module, snow physics and solar geometry are used to estimate all of the energy parameters, and the solar angle is derived from the topographic maps including slope and aspect maps obtained by using the Digital Elevation Model (DEM) and Geographic Information System (GIS) tools. Hence, the WEHY-HCM Snow Module simulates the snowmelt processes by taking the effect of topography into account. For this study, the Shuttle Radar Topographic Mission (SRTM) DEM with 3-arc-second (~90 m) resolution was downloaded from the USGS's website (https://lta.cr.usgs.gov/SRTM1Arc) and processed over the Gediz Basin (Fig. 5). The aspect and slope maps given in Fig. 6 were generated from the DEM and were used to measure solar radiation in the WEHY-HCM Snow Module. According to Ohara and Kavvas (2006), the aspect map is important in the spatial simulation of snow because the snow distribution on north-facing hillslopes is quite different from that on south-facing hillslopes. These maps are also used to obtain shortwave radiation without the cloud effect. The depth-averaged energy and mass conservation equations and the shortwave radiation are calculated by the model at each computational node and hence at each hillslope. As a result, the model takes the land surface energy estimates done at each node of a modeled watershed into account (Ohara and Kavvas, 2006). For the snowmelt process, the probability distribution function (PDF) method is employed to upscale from a single-layered point-scale snow model to a finite-scale model with the formulation of the Fokker-Planck

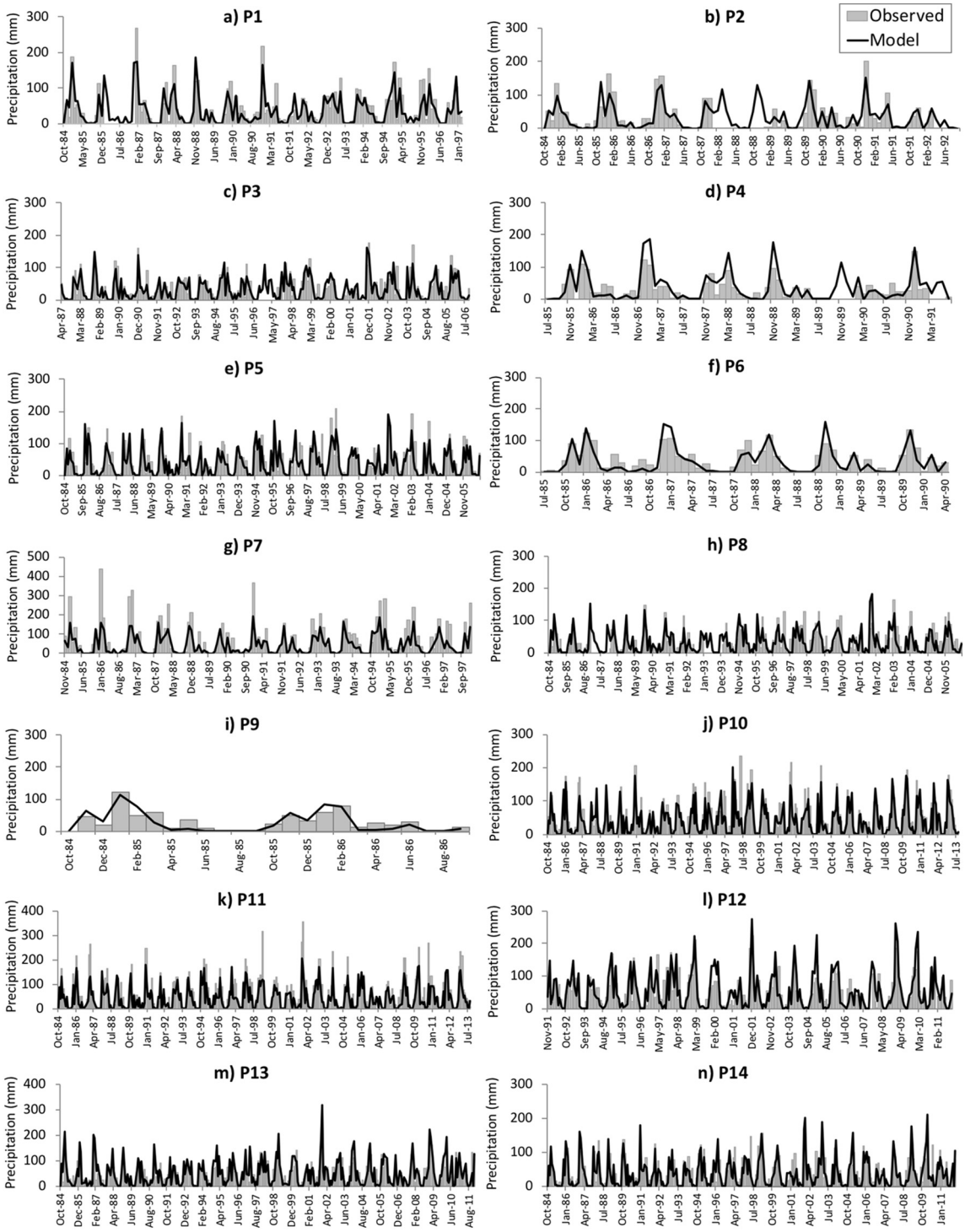

Fig. 4. Validation results for the WRF model showing the time series of the observed and simulated monthly precipitation values for all meteorological stations over the Gediz Basin.

equation (FPE). This method can even be applied for sparsely gauged or ungauged watersheds because the information on the statistical changes of atmospheric forcings (e.g. precipitation and shortwave radiation) in time and space can be included in the modeling process (Ohara et al., 2008).

In this study, the outputs of the WRF atmospheric model over the Gediz Basin were fed into the WEHY-HCM Snow Module as inputs to obtain the simulated values of the variables such as snow depth, snow-water equivalent, and snowmelt, among others. However, the Gediz Basin is a poorly gauged basin in terms of snow, which usually falls in mountainous, high-elevation regions of the basin in winter, and whose melting runoff contributes to the basin's streamflow. Snowmelt is usually not a significant source of water for the Demirkopru Reservoir because on average, snow cover stays on the ground for less than a few weeks. As the snow data recorded in the basin have too many missing values during the historical simulation period, the Snow Module could not be calibrated using the observed data. However, the simulated model results were compared against the satellite-observed snow cover data obtained from NASA's snow-cover datasets generated from Moderate Resolution Imaging Spectroradiometer (MODIS). Such

Table 3
Summary of the statistical properties of the observed and simulated monthly total precipitation for all meteorological stations in the Gediz Basin, and summary of the statistical test results performed for the validation of the WRF model simulations.

Station	Mean (mm)		Standard deviation (mm)		R	NSE
	Observed	Model	Observed	Model		
P1	42.17	36.51	48.45	41.33	0.89	0.77
P2	35.57	32.38	44.84	37.83	0.89	0.79
P3	34.65	32.56	35.99	33.85	0.86	0.73
P4	32.18	37.35	34.25	47.59	0.92	0.54
P5	40.92	38.18	43.81	41.64	0.83	0.67
P6	37.03	33.79	37.57	43.67	0.90	0.72
P7	68.80	43.01	84.71	49.24	0.88	0.59
P8	35.82	32.35	34.56	34.31	0.79	0.57
P9	28.34	26.49	29.83	33.34	0.91	0.78
P10	45.45	40.57	48.76	43.97	0.86	0.73
P11	56.99	43.28	64.10	47.06	0.87	0.69
P12	51.43	54.53	46.73	57.08	0.86	0.61
P13	45.86	49.55	39.80	51.67	0.86	0.54
P14	39.17	36.72	38.90	41.40	0.59	0.83

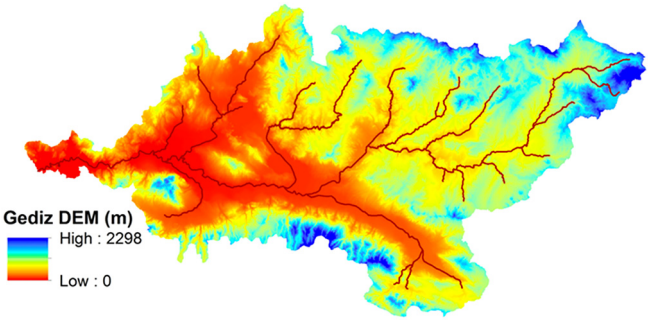

Fig. 5. Digital elevation map and stream network of the Gediz Basin.

comparisons from the beginning of two winter months (January and February) in 2012 are shown in Fig. 7. After obtaining results showing that the observed and simulated spatial distributions of snow accumulation were quite similar, the outputs of the Snow Module were then fed as inputs into the WEHY-HCM Watershed Hydrology Module.

2.2.2.2. The WEHY-HCM Hydrology Module. The WEHY Watershed Hydrology Module uses the outputs of the Snow Module as inputs. As a result, snowmelt processes are included in the streamflow forecasting of the WEHY-HCM. The land surface model component included in the hydrology module is comprised of five models describing the land surface hydrologic flow processes: 1) an atmospheric boundary layer model, which couples the land surface and the atmosphere, and enables the use of 6-km resolution atmospheric data provided by the innermost WRF model domain, 2) a heat balance model, which calculates the temperature of the top soil layer, 3) a vegetation model, which calculates precipitation interception by vegetation cover, 4) an evapotranspiration model, which calculates the evaporation from the bare soil and the evapotranspiration from the vegetated areas and 5) a soil water flow model, which computes infiltration and direct runoff (Kavvas et al., 2013).

In the Hydrology Module of the WEHY-HCM, the point-scale conservation equations for interception, infiltration, unsaturated flow, evapotranspiration, subsurface stormflow and overland flow at each individual slope of a watershed, interacting channel network and regional groundwater flow were upscaled to be able to use their ensemble-averaged forms. This approach allows the WEHY-HCM Model to take the effect of heterogeneity within natural watersheds into account in the computations. The model analyzes all model computational units (MCUs), or hillslopes, in parallel and simultaneously in terms of the surface and subsurface hillslope hydrologic processes. The model estimates the flowrate of water in the soil column at different soil depths as it infiltrates in the vertical direction, both within the soil root zone above the hardened soil layer beneath the plant roots as well as in the subsurface zone between the hardened layer and the groundwater table. Hence, the model computes the accretion rate for subsurface storm flow and deep groundwater recharge. The rainfall or snowmelt that is in excess is used by the overland flow component of the model as the lateral inflow flux. Thus, a portion of the infiltrated water into the soil becomes subsurface storm flow, another portion recharges the groundwater, and the remaining portion is stored in the soil column. Then, the flow discharges to the river system and the underlying unconfined groundwater aquifer of the watershed are computed dynamically at the MCUs, as there is an interaction between the surface and subsurface hillslope processes. The flow discharges coming from the hillslopes are finally routed via the river system and the unconfined aquifer throughout the watershed towards its outlet (Kavvas et al., 2013). In the case of the Gediz Basin, the outlet is where the Gediz River meets the Aegean Sea.

One of the advantages of the physically-based WEHY model is that the model parameters are based on basin's physical attributes/characteristics and/or field experiments. For this reason, the geomorphological parameters and the soil hydraulic parameters can be easily estimated from the existing geographical information system (GIS) datasets. As a result, the physically-based WEHY-HCM can be applied to ungauged or sparsely gauged watersheds, such as the Gediz Basin, and is adequate for the estimation of hydrologic extremes (Kure et al., 2013).

In this study, the unique parameter set including geomorphologic and soil hydraulic parameters required by the WEHY model was created or mapped by means of the DEM map, vegetation and land cover map, soil map, and other available data by using the ArcMap 10.1 program. Some of these parameters are provided in the Supplementary material (Fig. S1). The extraction of the stream network and the delineation of the MCUs were conducted by the HEC-GeoHMS program (HEC-GeoHMS, 2013), an ArcView based GIS tool. The reach network and MCUs were delineated as given in Fig. 8, where the Gediz Basin is

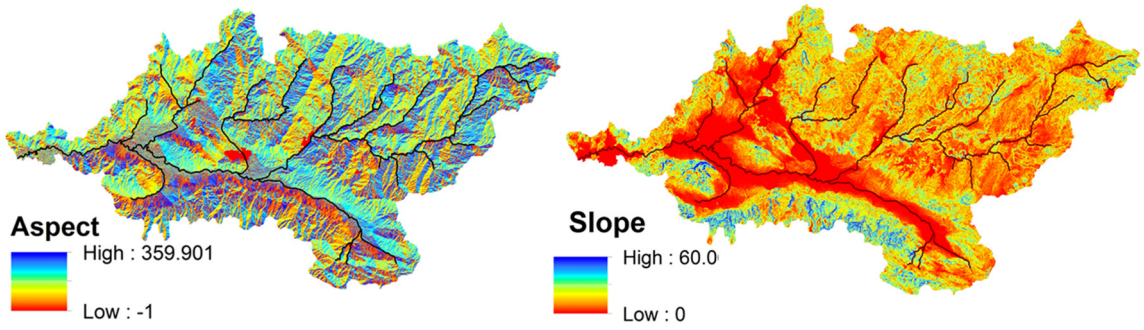

Fig. 6. Aspect and slope maps of the Gediz Basin.

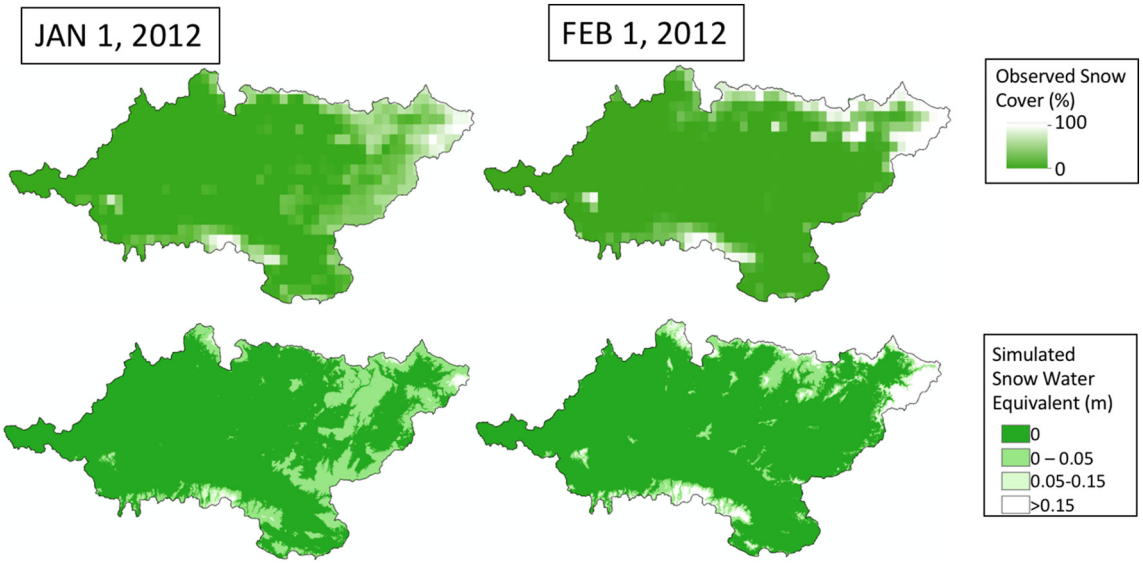

Fig. 7. Comparison of the satellite-observed snow cover percentage (top) against the model-simulated snow water equivalent (bottom) on January 1, 2012 and February 1, 2012 over the Gediz Basin.

shown to be subdivided into 138 MCUs. As for the vegetation cover and land use data, the Corine Land Cover (CLC) 2006 map with 100-m resolution (EEA, 2007) was used. Moreover, Leaf Area Index (LAI) data were obtained from MODIS datasets (MOD15A2 – Monthly), and their 10-year averages (2001—2010) for each month were computed over the Gediz Basin as shown in Fig. 9 and were used as an input to the WEHY Model. In addition, 1-km resolution soil depth data (the vertical distance between the soil surface and the bedrock or impervious layer) and soil texture data from different soil layers of the Gediz Basin were obtained from the International Soil Reference and Information Centre (ISRIC)'s World Soil Information (2013) (ISRIC, 2013). Finally, soil class properties were obtained for each MCU's soil texture class based on Mccuen et al. (1981) and Rawls et al. (1982) soil texture classifications for soil hydraulic parameters.

Following the configuration of the WEHY model and the preparation of the physical model parameters, calibration and validation were performed first with the dynamically-downscaled ERA-Interim reanalysis data to evaluate the model performance and also to reconstruct the almost nonexistent historical inflow data into the Demirkopru Reservoir. Since only 4-year long hydrological observed data (2009–2012) could be obtained from the Turkish General Directorate of State Hydraulic Works (DSI) under the aegis of the Ministry of Forest and Water Management, the observed flowrate data of the water years of 2009 and 2010 were used for model calibration, and of 2011 and 2012 were used for model validation. Moreover, since the time period of the observed hydrological data (2009–2012) lies in GCMs' future scenario period (2006–2100), the Hydrology Module of the WEHY-HCM was also calibrated and validated separately for each dynamically-downscaled GCM realization. According to Chen et al. (2011), dynamically downscaled data can be directly used to calibrate a hydrology model without bias correction, especially when the study basin is much larger than the horizontal resolution of the RCM. The assumption behind this method is

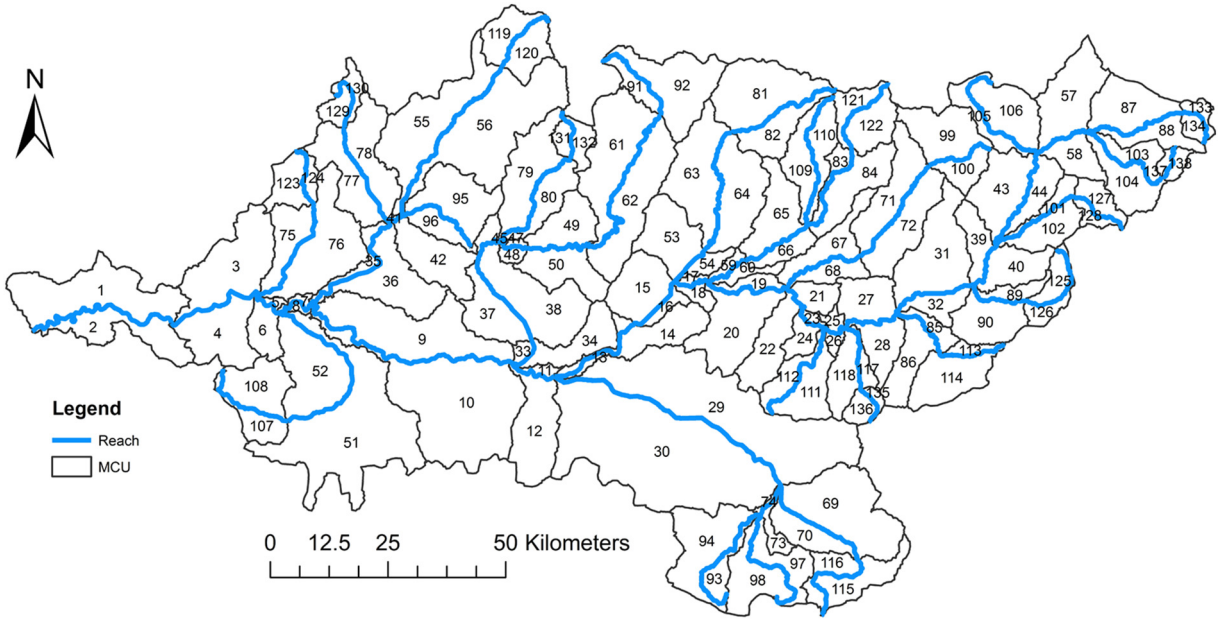

Fig. 8. Reach network and model computational units (MCUs) used for the hydrologic modeling of the Gediz Basin.

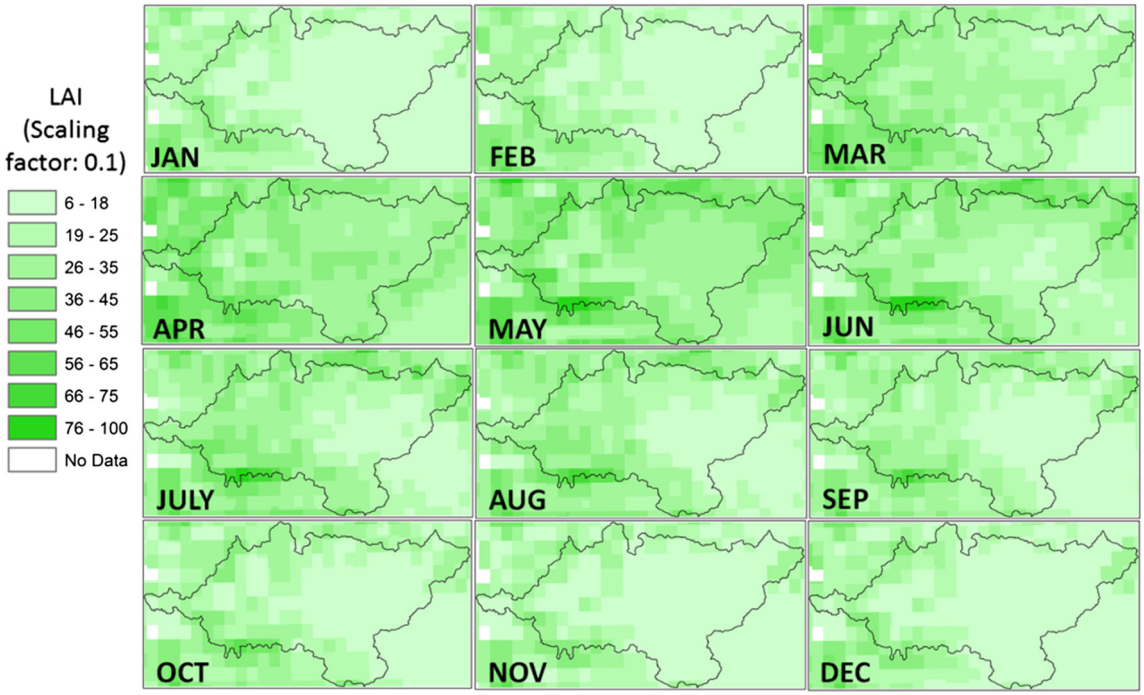

Fig. 9. 10-Year monthly averages of Leaf Area Index (LAI) data over the Gediz Basin.

that the dynamically downscaled data includes small biases that could be tackled by the hydrology model. In fact, if the hydrology model is calibrated by using realistic parameter values, and is able to represent the observed streamflows sufficiently, then it could be argued that the dynamically downscaled data do not include more bias than an observed dataset.

The locations of the three upstream flow gauging stations, whose data were compared against the simulated flowrate data during calibration and validation, are shown in Fig. 1. The calibration and validation results for the historical period, and for each of the future climate projections are given in Fig. 10, and a summary of the model statistics performed for each stream gauging station is shown in Table 4. In addition to R, the root-mean-square error (RMSE) was used to assess the model performance. Table 4 reveals high R values for calibration and validation of the model varying from 0.85 to 0.99. Moreover, the maximum RMSE values for stations F1, F2, and F3 are 7.62 m^3/s, 3.92 m^3/s, and 5.04 m^3/s, respectively, for the calibration period, and are 6.15 m^3/s, 1.94 m^3/s, and 2.19 m^3/s, respectively, for the validation period. Both Fig. 10 and Table 4 show that the model was able to match the observed average monthly streamflow data satisfactorily during the calibration period, and that it was also capable of adequately reproducing the observed average monthly streamflow data during the validation period as well for the historical reanalysis and the different future projections. The WEHY-HCM model configurations obtained by specifically calibrating the model for each GCM realization were then used to simulate the future runoff and reservoir inflows under climate change scenarios during the 21st century.

3. Results and discussion

3.1. Projected changes and trends in temperature

In this section the reconstructed historical basin average temperatures, obtained from the dynamical downscaling of the ERA-Interim reanalysis data, as well as the projected future temperatures under the eight different climate change projections, namely, HadGEM2-ES RCP4.5, HadGEM2-ES RCP8.5, MIROC5 RCP4.5, MIROC5 RCP 8.5, GFDL-ESM2M RCP4.5, GFDL-ESM2M RCP8.5, CCSM4 RCP4.5, and CCSM4 RCP8.5, are presented and discussed. The historical temperatures were reconstructed for the period of 28 years (1985–2012) and were used as a reference to assess and quantify the expected changes under the future climate change projections, which were performed for an 84-year period from 2017 to 2100.

The time series of the annual average temperatures for all GCM projections during the future period, along with their ensemble average time series are presented in Fig. 11(a). In addition, 10-year moving averages of all the time series given in Fig. 11(a) are shown in Fig. 11(b). It is clear from Fig. 11(a) that the annual average temperatures of the ensemble of all projections are generally projected to follow an increasing trend throughout the 21st century. These projected increases in temperature under RCP4.5 and RCP8.5 scenarios over the 21st century agree with the Fifth Assessment Report of the IPCC (IPCC, 2014). The individual projections also show a similar trend in the annual average temperature, however with a greater fluctuation within each projection and with a greater variability among the different projections. The projected increasing trend in the annual average temperature is also seen in Fig. 11(b), in which the variability is dampened due to the 10-year averaging effect. It is clear from Fig. 11(b) that the projections expected to have the highest temperatures by the end of the century are CCSM4 RCP8.5, HadGEM2-ES RCP8.5 and MIROC5 RCP8.5, whereas the projection expected to have the lowest temperatures is GFDL-ESM2M RCP4.5.

In order to see how the projected basin-scale temperature for each month compares to the historical values, the average monthly temperatures for the historical period and for the ensemble average of the eight GCM projections for the future period (2017–2100) are plotted in Fig. 12. This figure also includes the 90% confidence band for the ensemble average of the projected temperatures. It is clear in this figure that the historical average monthly temperatures fall within the confidence interval of the future projection, but much closer to the lower end of the interval and below the line of the ensemble of the projections. Therefore, the average monthly temperatures for the ensemble average of the projections are projected to be greater than their historical counterparts for all of months of the year, the smallest difference being +0.3 °C,

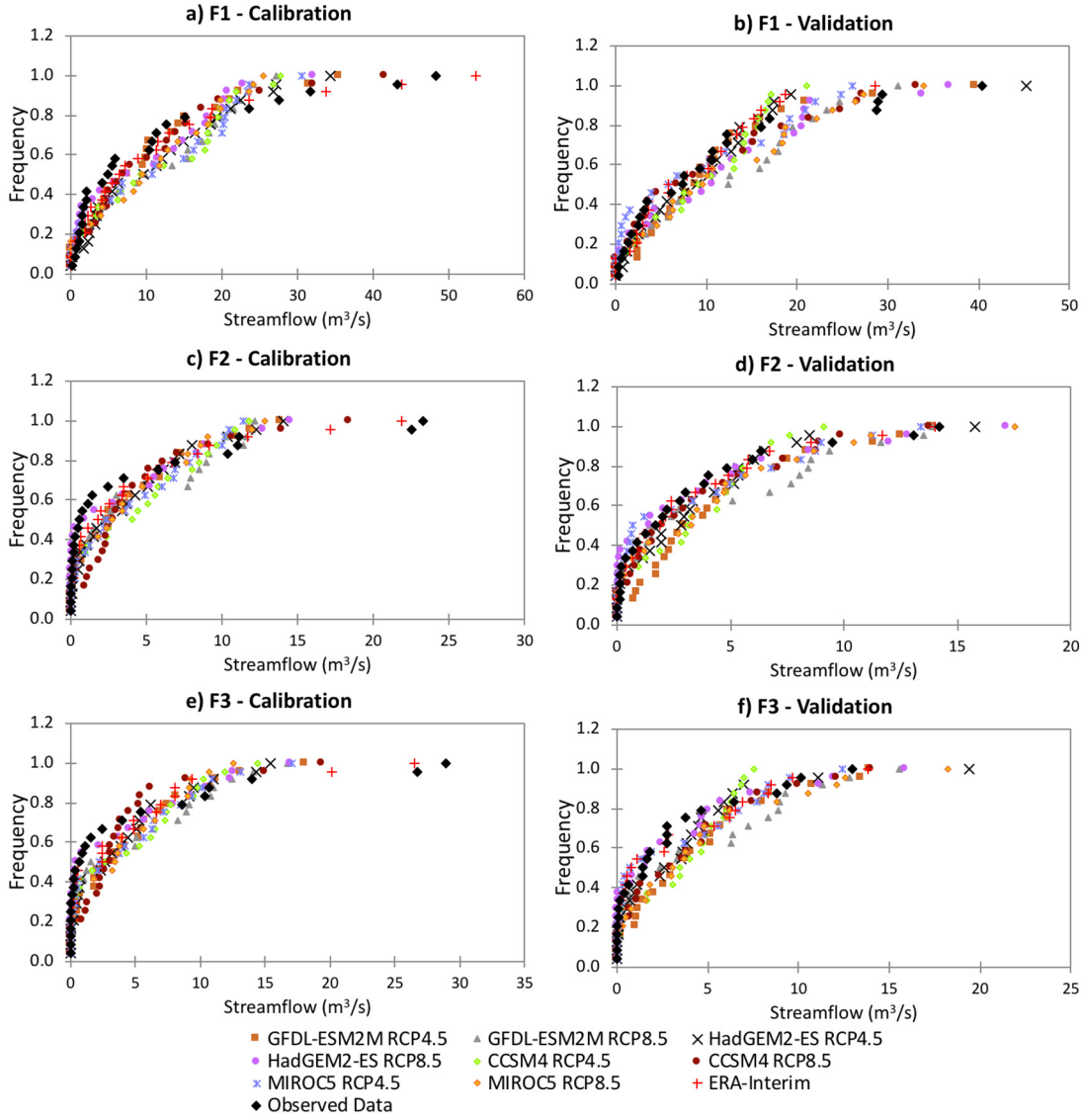

Fig. 10. Comparisons of the observed average monthly streamflow and the corresponding simulated streamflow at the different stream gauging stations for the calibration and validation of the WEHY model over the Gediz Basin.

expected in October, and the largest difference being +2.5 °C, expected in July. Moreover, the width of the 90% confidence interval ranges between 2.1 °C (in December) and 6.6 °C (in July), again revealing the large uncertainty and variability among the different climate projections. In fact, the confidence band indicates that the uncertainty is largest during the summer months, and smallest in the winter months. This is consistent with other studies (Cattiaux et al., 2013; Sillmann et al., 2013) carried out using CMIP5 GCM outputs that have shown that summer warming is expected to be larger than winter warming especially over the Mediterranean region. Similarly, Hertig and Jacobeit

Table 4
Summary of the statistical test results performed for stream gauging stations for the calibration and validation of the Hydrology Module of the WEHY-HCM (The unit of RMSE is m^3/s).

	F1 (Gediz)				F2 (Delinis)				F3 (Demirci)			
	Calibration		Validation		Calibration		Validation		Calibration		Validation	
	R	RMSE	R	RMSE	R	RMSE	R	RMSE	R	RMSE	R	RMSE
GFDL-ESM2M RCP4.5	0.98	4.67	0.97	3.14	0.93	3.28	0.98	1.43	0.93	3.98	0.97	1.73
GFDL-ESM2M RCP8.5	0.86	7.62	0.93	4.39	0.86	3.60	0.95	1.88	0.90	4.06	0.95	2.19
HadGEM2-ES RCP4.5	0.94	5.54	0.92	4.24	0.94	3.24	0.95	1.25	0.94	4.05	0.93	1.72
HadGEM2-ES RCP8.5	0.91	6.53	0.95	3.74	0.95	2.91	0.99	0.97	0.93	3.89	0.98	1.03
CCSM4 RCP4.5	0.87	7.28	0.88	6.15	0.85	3.92	0.90	1.94	0.87	4.72	0.85	2.08
CCSM4 RCP8.5	0.98	4.10	0.98	2.38	0.97	2.59	0.96	1.13	0.97	3.84	0.97	1.35
MIROC5 RCP4.5	0.87	7.13	0.94	4.19	0.87	3.86	0.97	1.04	0.92	4.10	0.96	1.08
MIROC5 RCP8.5	0.88	7.36	0.96	3.58	0.93	3.38	0.97	1.36	0.87	5.04	0.99	1.91
ERA Interim	0.99	2.28	0.96	4.78	0.98	1.48	0.99	0.47	0.98	2.11	0.97	0.92

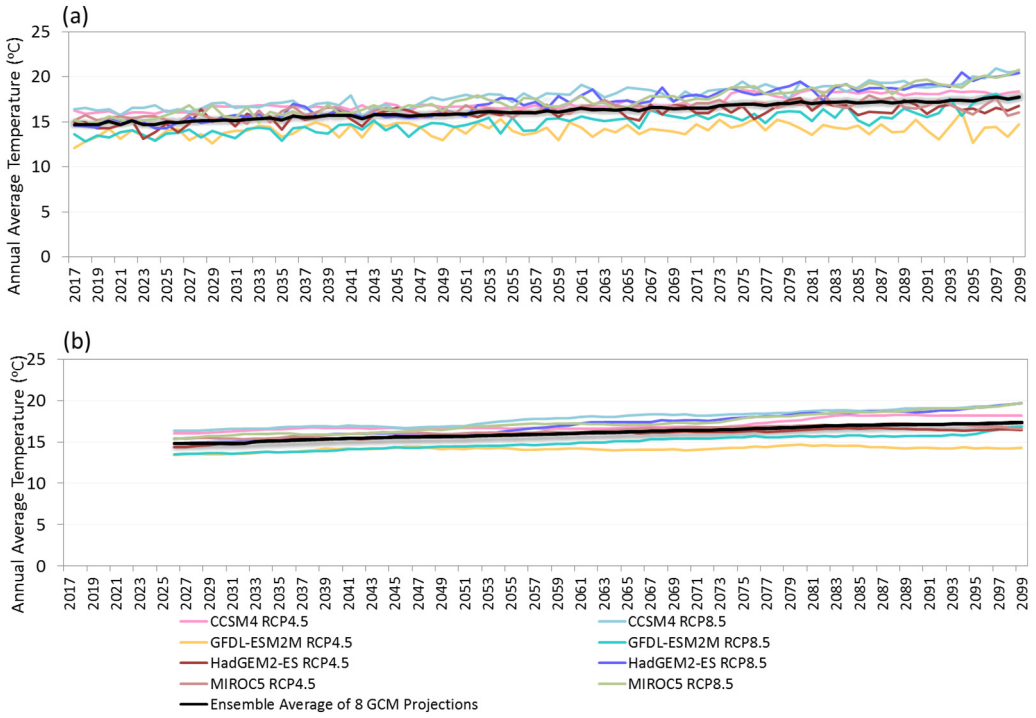

Fig. 11. Plots of (a) the projected annual average temperatures and (b) their corresponding 10-yr moving averages, during the future period of the 21st century for all the eight different climate projections and for their ensemble average.

(2008) assessed Mediterranean temperature changes under the Special Report on Emission Scenarios (SRES) scenarios and showed an increase in temperature for all months of the year in the period 2071–2100 compared to 1990–2019, varying between 2 °C and 4 °C, depending on region and season.

Statistical analysis results of the annual average temperatures are given in Table 5. For comparison purposes, the 21st century is analyzed in 4 different periods in this table. The period from 2017 to 2044 (28 years) is defined as the early century; the period from 2045 to 2072 (28 years) is defined as the mid-century; and the period from 2073 to 2100 (28 years) is defined as the late century. In addition to these, the results are also presented for the entire 21st century (2017–2100) for 84 years. Historical temperatures are also given for a 28-year period for the years between 1985 and 2012. In this table, the minimum, maximum, standard deviation and the mean of the annual average temperatures are provided for each time period. The average annual temperatures for each future time period are compared to the historical mean temperature (15.3 °C) over the Gediz Basin, and the changes in the projected average annual temperatures in comparison to the historical counterpart are also provided in the table.

From this table, it can be seen that the average annual temperature for different climate projections may be either higher or lower than the historical values, depending on the GCM and the RCP involved. For example, the average annual temperature of GFDL-ESM2M RCP4.5 is projected to be lower than the historical average throughout early, mid-, and late century, and is in fact the lowest among all other projections (a result which was also deduced from Fig. 11). On the other hand, CCSM4 RCP8.5 is projected to have the largest increase in average annual temperature for all three periods, as compared to the historical value. Moreover, the change in the average annual temperatures of the future projections of each GCM is generally greater, or more positive, for RCP8.5 scenarios compared to their corresponding RCP4.5 scenarios, revealing higher projected temperatures for RCP8.5 scenarios throughout the century. This may be explained by the fact that the RCP8.5 is a very high baseline scenario which does not include any mitigation measures, whereas RCP4.5 is an intermediate stabilization emission scenario. Furthermore, note that due to the uncertainty among the GCMs and the variability among the RCPs, the expected change in average annual temperature, as compared to the historical value, is projected to vary between −1.5 and 1.3 °C in the early century, −1.2 and 2.6 °C in mid-century, −0.9 and 3.9 °C in the late century. However, considering the ensemble average of all projections for these three periods, the average annual temperature is expected to be the same as that of the historical period for the early century, while it is expected to exceed the historical value by 1.1 °C in the mid-century, and 2.2 °C in the late century. According to the projections from the EURO-CORDEX initiative (EEA, 2017), multi-model ensemble mean temperatures across Europe, which includes the Northern Mediterranean region and Turkey, are expected to warm in the range of 1 to 4.5 °C under the RCP4.5 scenario and in the range of 2.5 to 5.5 °C under RCP8.5 over the

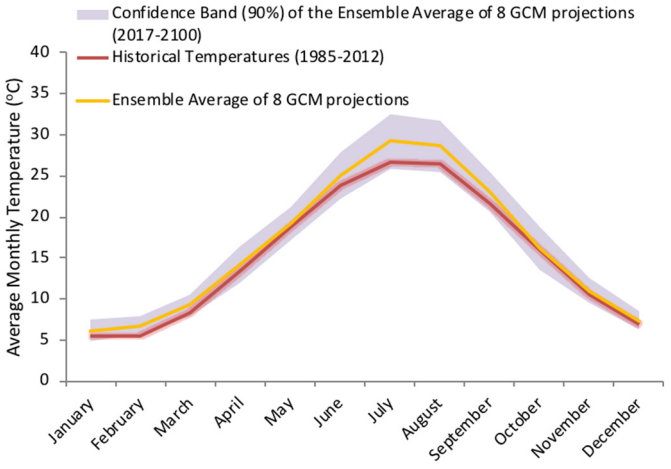

Fig. 12. Plots of the average monthly temperatures for the historical period (1985–2012), and the ensemble average monthly temperatures for the future period (2017–2100) along with their 90% confidence band.

Table 5
Statistical results of the basin-scale temperatures for the historical period and the three future periods, based on the annual average temperature time series.

	Annual average temperature (°C)				Change compared to the historical period (°C)	Annual average temperature time series	
	Min	Max	Stdev	Mean		Trend	p-Value
Historical temperatures (1985–2012) (28 years)	14.1	16.6	0.6	15.3	–	**Increase**	**0.010**
Early century (2017–2044) (28 years)							
CCSM4 – RCP4.5	15.8	17.0	0.4	16.4	1.1	**Increase**	**0.000**
CCSM4 – RCP8.5	15.5	18.0	0.5	16.6	1.3	**Increase**	**0.010**
GFDL-ESM2M – RCP4.5	12.1	15.0	0.7	13.8	−1.5	**Increase**	**0.003**
GFDL-ESM2M – RCP8.5	12.8	15.1	0.6	13.8	−1.5	**Increase**	**0.000**
HadGEM2-ES – RCP4.5	13.1	16.4	0.8	15.1	−0.2	**Increase**	**0.005**
HadGEM2-ES – RCP8.5	14.3	17.0	0.7	15.4	0.1	**Increase**	**0.000**
MIROC5 – RCP4.5	14.8	16.7	0.5	15.7	0.4	**Increase**	**0.010**
MIROC5 – RCP8.5	14.7	16.9	0.6	15.8	0.5	**Increase**	**0.001**
Ensemble average (8 projections)	14.6	16.0	0.4	15.3	0	**Increase**	**0.000**
Mid-century (2045–2072) (28 years)							
CCSM4 – RCP4.5	16.0	17.4	0.3	16.7	1.4	Decrease	0.980
CCSM4 – RCP8.5	16.2	19.1	0.7	17.9	2.6	**Increase**	**0.000**
GFDL-ESM2M – RCP4.5	12.9	15.3	0.6	14.1	−1.2	Decrease	0.420
GFDL-ESM2M – RCP8.5	13.3	16.3	0.7	15.0	−0.3	**Increase**	**0.000**
HadGEM2-ES – RCP4.5	15.2	16.9	0.4	16.1	0.8	Increase	0.240
HadGEM2-ES – RCP8.5	15.5	18.8	0.9	17.0	1.7	**Increase**	**0.000**
MIROC5 – RCP4.5	15.5	17.4	0.5	16.4	1.1	**Increase**	**0.000**
MIROC5 – RCP8.5	16.2	17.9	0.5	17.2	1.9	**Increase**	**0.046**
Ensemble average (8 projections)	15.7	17.0	0.3	16.4	1.1	**Increase**	**0.000**
Late century (2073–2100) (28 years)							
CCSM4 – RCP4.5	16.7	18.6	0.4	18.2	2.9	Increase	0.870
CCSM4 – RCP8.5	17.5	20.9	0.7	19.2	3.9	**Increase**	**0.000**
GFDL-ESM2M – RCP4.5	12.7	16.1	0.7	14.4	−0.9	Decrease	0.140
GFDL-ESM2M – RCP8.5	14.6	18.1	0.9	16.1	0.8	**Increase**	**0.003**
HadGEM2-ES – RCP4.5	15.3	17.7	0.6	16.5	1.2	Decrease	0.840
HadGEM2-ES – RCP8.5	17.3	20.5	0.7	19.0	3.7	**Increase**	**0.000**
MIROC5 – RCP4.5	15.7	18.0	0.6	16.9	1.6	Decrease	0.110
MIROC5 – RCP8.5	18.0	20.7	0.7	19.0	3.7	**Increase**	**0.000**
Ensemble average (8 projections)	16.9	18.5	0.4	17.5	2.2	**Increase**	**0.000**
21st century (2017–2100) (84 years)							
CCSM4 – RCP4.5	15.8	18.6	0.8	17.1	1.8	**Increase**	**0.000**
CCSM4 – RCP8.5	15.5	20.9	1.2	17.9	2.6	**Increase**	**0.000**
GFDL-ESM2M – RCP4.5	12.1	16.1	0.7	14.1	−1.2	**Increase**	**0.005**
GFDL-ESM2M – RCP8.5	12.8	18.1	1.2	15.0	−0.3	**Increase**	**0.000**
HadGEM2-ES – RCP4.5	13.1	17.7	0.9	15.9	0.6	**Increase**	**0.000**
HadGEM2-ES – RCP8.5	14.3	20.5	1.7	17.1	1.8	**Increase**	**0.000**
MIROC5 – RCP4.5	14.8	18.0	0.7	16.3	1	**Increase**	**0.000**
MIROC5 – RCP8.5	14.7	20.7	1.5	17.3	2	**Increase**	**0.000**
Ensemble average of four RCP4.5 scenarios	14.5	17.0	0.6	15.8	0.5	**Increase**	**0.000**
Ensemble average of four RCP8.5 scenarios	14.6	19.9	1.3	16.8	1.5	**Increase**	**0.000**
Ensemble average of 8 GCM projections	14.7	18.2	0.9	16.3	1	**Increase**	**0.000**

period from 2071 to 2100 compared to the baseline period from 1971 to 2000. Moreover, Zanis et al. (2015) performed 10-km resolution dynamical downscaling over Greece for the period from 1960 to 2100 under a SREC scenario (A1B). It was found that the annual land surface temperatures increased by less than 1.8 °C for the period from 2021 to 2050, and by about 3.4 to 4.2 °C for the period from 2071 to 2100 compared to that of the historical period.

When considering the changes in the average annual temperature over the entire 21st century, similar results can be seen. In fact, among all the GCM projections, only the projections of GFDL-ESM2M GCM have annual average temperatures lower than that of the historical period. Moreover, the change in the average annual temperature is expected to be the most positive under CCSM4 RCP8.5 (+2.6 °C), and the most negative under GFDL-ESM2M RCP4.5 (−1.2 °C). Furthermore, it can again be seen that the expected change in average annual temperature for the ensemble average of the four RCP8.5 scenarios is greater (+1.5 °C) than that of RCP4.5 (+0.5 °C). Finally, the ensemble of all eight GCM projections shows an average annual temperature greater than the historical value when considered for the whole 21st century.

The last two columns of Table 5 show the results of the trend analysis test for the annual average temperature time series. For this purpose, the non-parametric Mann Kendall test at 95% confidence level is employed to detect the trends in each time period as well as in the entire century, and the statistically significant trends are given in bold color. The results of the trend analysis indicate that the annual average temperature time series for the early century have statistically significant increasing trends for all GCM projections. Moreover, all increasing trends in the mid- and late centuries are statistically significant, while none of the decreasing trends are found to be statistically significant. When the results of the entire 21st century are evaluated, it is found that all GCM realizations indicate that a significant increase in the annual average temperatures is expected throughout the 21st century, a result which was also graphically clear from Fig. 11(a) and (b).

3.2. Projected changes and trends in reservoir inflows

After creating the historical and future climatic conditions under eight different future climate projections as described in Section 2.2.1

and analyzed in Section 3.1, these outputs were then fed into the Snow Module and Hydrology Module of the WEHY-HCM model for the same future time period (2017–2100) to simulate the inflows into the Demirkopru Reservoir, which is located in the upper Gediz Basin. The timing and magnitude of these inflows determine how much water will be stored in this largest reservoir and main storage structure of the basin for the irrigation season. The analysis of the projected monthly and annual reservoir inflows will be presented and discussed below.

The projected monthly average flowrates under eight climate projections are given in Fig. 13(a)–(d). From these plots, it is clear that the RCP4.5 scenarios produce larger reservoir inflows, and sometimes larger peak flows, than the RCP8.5 scenarios under the CCSM4 and GFDL-ESM2M GCMs. However, the reservoir inflows projected by the HadGEM2-ES and MIROC5 GCMs are more or less the same among the two RCPs. Fig. 13(e) illustrates the ensemble average of all eight climate projections, along with the 90% confidence band. This plot shows that

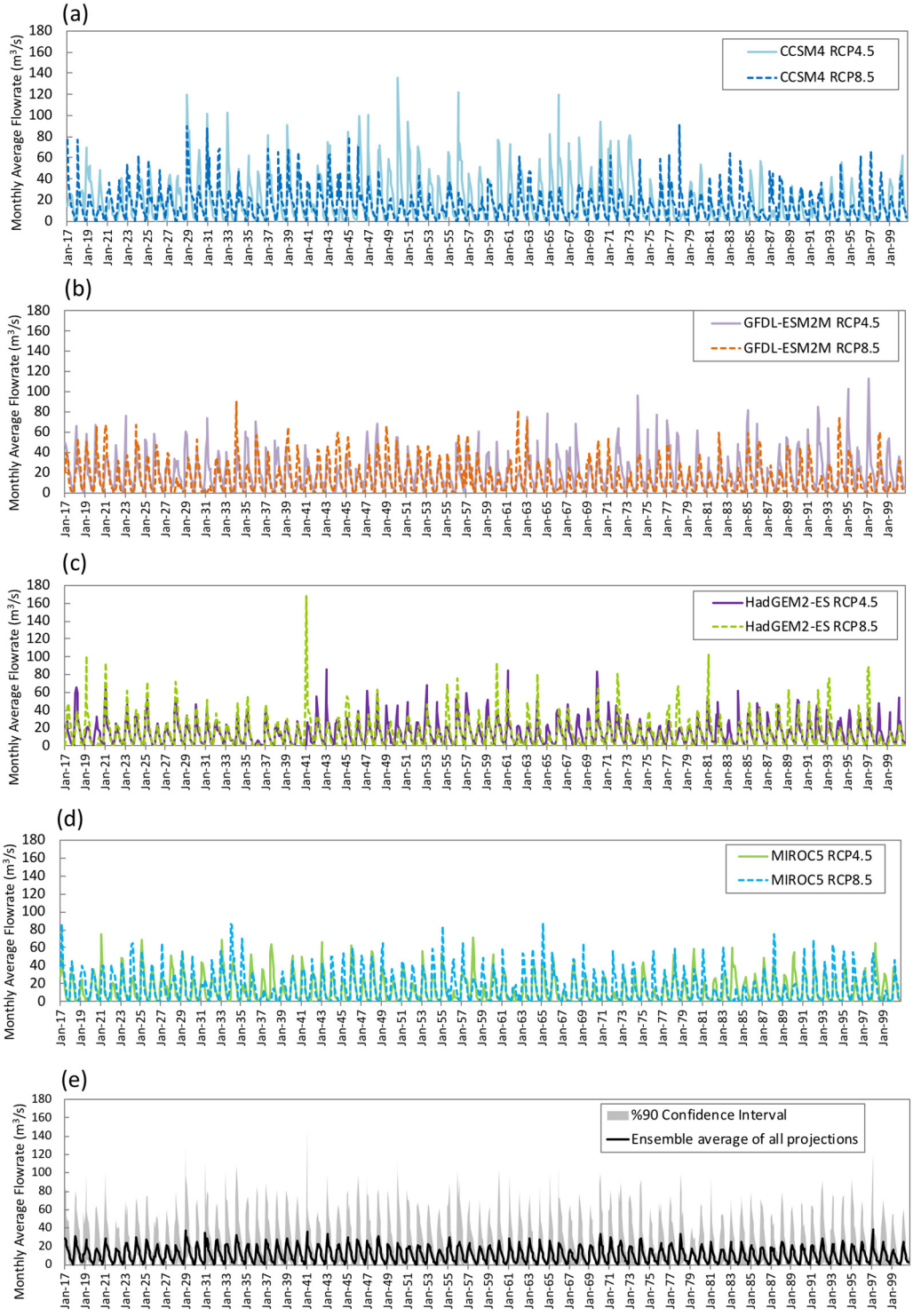

Fig. 13. Time series of the projected monthly average inflows into the Demirkopru Reservoir obtained for the (a) CCSM4, (b) GFDL-ESM2M, (c) HadGEM2-ES, and (d) MIROC5 climate projections. The ensemble average of all projections along with their 90% confidence interval is given in (e).

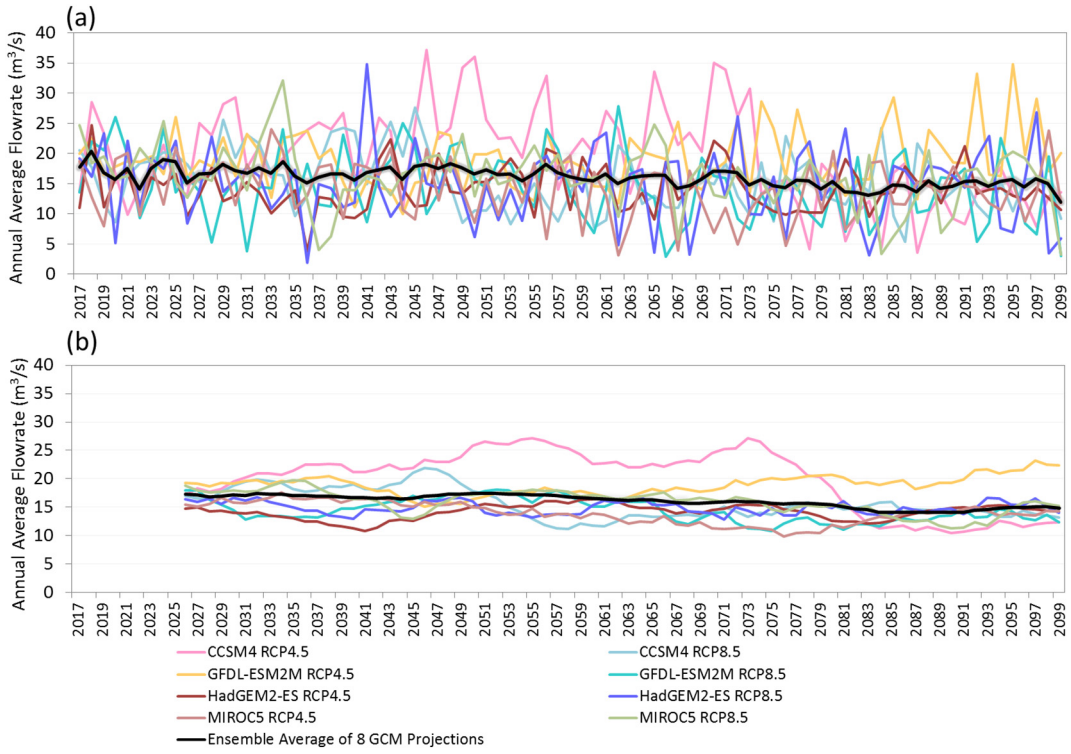

Fig. 14. Plots of (a) the projected annual average inflows into the Demirkopru Reservoir and (b) the their corresponding 10-yr moving averages, during the future period of the 21st century for all the eight different climate projections and for their ensemble average.

the monthly simulated inflows show a large variability, especially for the peak flow months, which can be attributed to the model uncertainty and RCP variability.

Fig. 14(a) represents the time series of the projected annual average reservoir inflows under the eight future climate projections, along with their ensemble average time series. The 10-year moving averages of all these time series are provided in Fig. 14(b). Fig. 14(a) indicates a large variability in the projected annual average inflows among all eight climate projections. In fact, it is clear from the plot that CCSM4 RCP4.5 shows the greatest variability among the climate projections, which was found to have a standard deviation that is up to 1.6 times larger than the other projections. While a trend in reservoir inflows is not directly obvious from the individual climate change projections and their large fluctuations shown on Fig. 14(a), the ensemble average of all eight projections shows a clear downward trend throughout the 21st century. Similarly, a downward trend in the reservoir inflows is also visible from the 10-year moving average of the ensemble of all projections, as shown in Fig. 14(b). However, Fig. 14(b) reveals that projected inflows for GFDL-ESM2M RCP4.5 scenario increase throughout the 21st century, and are expected to sustain the highest reservoir inflows by the end of the century.

In order to see how the projected reservoir inflows for each month compare to the corresponding historical values, the average monthly reservoir inflows for the historical period and for the ensemble average of the eight climate projections for the future period are plotted in Fig. 15. This figure also shows the 90% confidence band for the ensemble average of the projected inflows. Fig. 15 shows that the historical average monthly inflows fall within the confidence interval of the future projections and are similar to those of the ensemble average. However, the latter are slightly larger than the former for all months. As such, the average monthly reservoir inflows for the ensemble average of the eight climate projections are projected to be greater than their historical counterparts for all months, the smallest difference being 0.16 m^3/s, expected in July, and the largest difference being 5.31 m^3/s, expected in January. Moreover, according to the 90% confidence band, the winter months (December–January–February) show the intervals of the largest possible average monthly inflows, thus revealing the greatest variability and uncertainty of reservoir inflows during these winter months. This implies that the choice of the GCM projection has a great impact on the winter inflows into the Demirkopru Reservoir, and eventually will have a great impact on the projected available water for irrigation in the Gediz Basin. This is because a significant portion of these winter flows is stored in the Demirkopru Reservoir and are then released during the irrigation season in summer.

The statistical analysis results of the monthly and annual average reservoir inflows for the historical period and the future period are given in Table 6. These inflows are analyzed with 28-year time periods for the historical period (1985–2012), early century (2017–2044), mid-century (2045–2072), and late century (2073–2100). In addition to these periods, statistical results are also presented for the entire

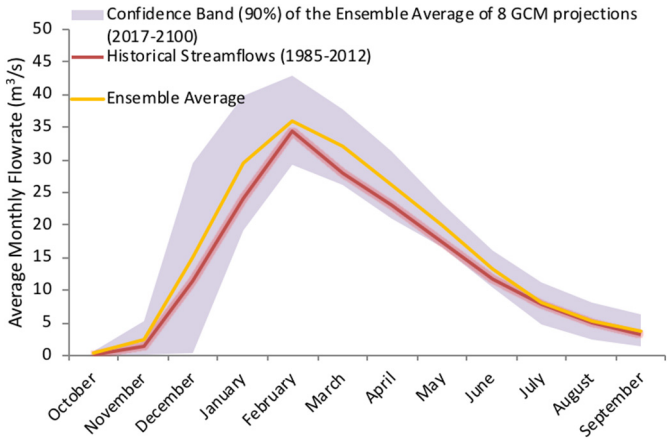

Fig. 15. Plots of the average monthly inflows into the Demirkopru Reservoir for the historical period (1985–2012), and the ensemble average monthly inflows for the future period (2017–2100) along with their 90% confidence band.

Table 6
Statistical results of the inflows into the Demirkopru Reservoir for the historical period and the three future periods, based on the monthly and annual average flowrate time series.

	Monthly average flowrate (m^3/s)				Average annual inflow volume (MCM)	Change compared to the historical inflow (%)	Annual average flowrate time series	
	Min	Max	Stdev	Mean			Trend	p-Value
Historical streamflow (1985–2012) (28 years)	0.0	90.4	14.0	13.8	433.4	–	Increase	0.19
Early century (2017–2044) (28 years)								
CCSM4 – RCP4.5	0.0	119.5	20.8	20.3	637	47.0	Increase	0.20
CCSM4 – RCP8.5	0.0	89.4	16.4	18.5	581	34.1	Increase	0.12
GFDL-ESM2M – RCP4.5	0.0	75.9	15.7	18.4	576	32.9	Decrease	0.09
GFDL-ESM2M – RCP8.5	0.0	90.8	17.2	15.8	496	14.4	Decrease	0.83
HadGEM2-ES – RCP4.5	0.0	85.4	13.3	13.7	425	−1.9	Decrease	0.33
HadGEM2-ES – RCP8.5	0.0	168.4	18.1	15.4	479	10.5	Decrease	0.09
MIROC5 – RCP4.5	0.0	75.2	16.1	16.0	500	15.4	No trend	1.00
MIROC5 – RCP8.5	0.0	86.7	17.3	17.3	541	24.8	Decrease	0.09
Ensemble average (8 projections)	0.0	48.0	12.9	16.9	530	22.3	Decrease	0.30
Mid-century (2045–2072) (28 years)								
CCSM4 – RCP4.5	0.0	136.2	26.0	25.4	797	83.9	Decrease	0.65
CCSM4 – RCP8.5	0.0	80.6	12.6	13.9	436	0.6	Increase	0.74
GFDL-ESM2M – RCP4.5	0.0	78.7	15.2	18.1	570	31.5	Increase	0.86
GFDL-ESM2M – RCP8.5	0.0	81.5	16.0	14.9	469	8.2	Decrease	0.08
HadGEM2-ES – RCP4.5	0.0	84.7	14.6	15.4	478	10.3	Increase	0.37
HadGEM2-ES – RCP8.5	0.0	93.3	16.5	15.0	467	7.8	Increase	0.74
MIROC5 – RCP4.5	0.0	71.0	14.2	12.6	394	−9.1	Decrease	0.15
MIROC5 – RCP8.5	0.0	87.0	16.9	17.0	530	22.3	Decrease	0.30
Ensemble average (8 projections)	0.0	54.0	13.0	16.5	518	19.5	Decrease	0.20
Late century (2073–2100) (28 years)								
CCSM4 – RCP4.5	0.0	81.7	15.0	13.1	397	−8.4	Decrease	0.50
CCSM4 – RCP8.5	0.0	91.3	13.7	14.4	448	3.4	Decrease	0.43
GFDL-ESM2M – RCP4.5	0.0	112.5	19.1	20.7	653	50.7	Increase	0.38
GFDL-ESM2M – RCP8.5	0.0	73.8	14.6	12.5	390	−10.0	Increase	0.83
HadGEM2-ES – RCP4.5	0.0	61.4	12.1	13.6	419	−3.3	Increase	0.20
HadGEM2-ES – RCP8.5	0.0	101.8	16.5	14.0	439	1.3	Decrease	1.00
MIROC5 – RCP4.5	0.0	64.5	14.6	13.7	424	−2.2	Increase	0.38
MIROC5 – RCP8.5	0.0	74.6	15.6	14.1	436	0.6	Increase	0.53
Ensemble average (8 projections)	0.0	51.1	11.7	14.5	451	4.1	Increase	0.26
21st century (2017–2100) (84 years)								
CCSM4 – RCP4.5	0.0	136.2	21.7	19.6	613	41.4	**Decrease**	**0.00**
CCSM4 – RCP8.5	0.0	91.3	14.5	15.6	488	12.6	**Decrease**	**0.01**
GFDL-ESM2M – RCP4.5	0.0	112.5	16.8	19.1	597	37.7	Increase	0.37
GFDL-ESM2M – RCP8.5	0.0	90.8	16.0	14.4	451	4.1	**Decrease**	**0.02**
HadGEM2-ES – RCP4.5	0.0	85.4	13.4	14.2	440	1.5	Increase	0.78
HadGEM2-ES – RCP8.5	0.0	168.4	17.1	14.8	460	6.1	Decrease	0.53
MIROC5 – RCP4.5	0.0	75.2	15.1	14.1	440	1.5	**Decrease**	**0.04**
MIROC5 – RCP8.5	0.0	87.0	16.7	16.1	503	16.1	**Decrease**	**0.03**
Ensemble average of four RCP4.5 scenarios	0.0	63.3	13.5	16.7	523	20.7	**Decrease**	**0.01**
Ensemble average of four RCP8.5 scenarios	0.0	57.7	12.9	15.2	476	9.8	**Decrease**	**0.00**
Ensemble average of 8 GCM projections	0.0	54.0	12.6	16.0	500	15.4	**Decrease**	**0.00**

21st century from 2017 through 2100 (84 years). In Table 6, minimum, maximum, standard deviation and the mean of the monthly average inflows are provided for each time period. These results show that for all future periods, the means of the monthly average flowrates of the ensemble average of all scenarios are greater than that of the historical period.

Table 6 also provides the average annual inflow volumes in million cubic meters (MCM) and their percentage changes compared to their historical counterpart (433.4 MCM). During the early century, the average annual inflow volume is expected to exceed the historical value for all the climate projections (+10.5% to +47.0%) except for HadGEM2-ES RCP4.5, whose inflow volume is expected to decrease by 1.9% compared to the historical inflows. In the mid-century, only MIROC5 RCP4.5 is projected to have a decrease in its average annual inflow volume as compared to the historical period (−9.1%), with the remaining climate projections showing an increase between 0.6% and 83.9%. As for the late century, the average annual inflow volumes corresponding to the projections GFDL-ESM2M RCP8.5, CCSM4 RCP4.5, HadGEM2-ES RCP4.5 and MIROC5 RCP4.5 are projected to decrease by 10%, 8.4%, 3.3% and 2.2%, respectively, while they are expected to increase by 0.6% to 50.7% for the remaining four projections. In the cases of the ensemble averages of the eight climate projections, the inflow volumes are expected to increase by 22.3%, 19.5% and 4.1% in the early century, mid-century and the late century, respectively. However, it is clear that these changes become less positive with time throughout the 21st century. It is interesting to note, though, that the projection whose average annual inflow volume is expected to exceed the historical value for all three periods and to have the second highest increase in the inflow for the whole 21st century (GFDL-ESM2M RCP4.5), is the same projection that is expected to have the lowest average annual temperature for all three periods and for the whole 21st century.

When considering the changes in the average annual inflow volume over the entire 21st century, the inflow volumes for all eight climate projections are expected to exceed those of the historical period, by 1.5% to 41.4% depending on the projection. The change in the average annual inflow volume is expected to be the greatest under the CCSM4 RCP4.5 projection, and the smallest under the MIROC5 RCP4.5 projection. Moreover, the change in the average annual inflow volume for the ensemble average of the four RCP4.5 scenarios is projected to be greater (+20.7%) than that of the RCP8.5 scenarios (+9.8%). Finally,

when considering the ensemble average of all projections throughout the entire century, the average annual reservoir inflow is projected to exceed the historical value by 15.4%. It is interesting to note, however, that the ensemble of scenarios projected to have the highest increase in average annual reservoir inflow (i.e., RCP4.5 scenarios) are the ones projected to have the lowest increase in the average annual temperature (see Table 5).

The last two columns in Table 6 provide the results of the trend analyses for the annual average reservoir inflow time series. The trend analyses are carried out using the non-parametric Mann-Kendall test at 95% confidence level, where the statistically significant trends are shown in bold. According to the results, none of the increasing and decreasing trends in the annual average flowrate occurring in early, mid-, and late century are statistically significant. However, considering the inflows over the whole 21st century, the downward trends obtained under CCSM4 RCP4.5, CCSM4 RCP8.5, GFDL-ESM2M RCP8.5, MIROC5 RCP4.5 and MIROC5 RCP8.5 are found to be statistically important. In addition, the ensemble average of the four RCP4.5 projections, the ensemble average of the four RCP8.5 projections, and the ensemble average of the eight climate projections all show statistically significant decreasing trends throughout the century. Therefore, even though the volume of reservoir inflows over the 21st century is projected to exceed the historical value on average, these individual annual reservoir inflows are expected to follow a decreasing trend with time throughout the century.

4. Summary and conclusions

In this study, the impact of future climate change on the hydroclimatology of the Gediz Basin, a Mediterranean agriculture-dominant basin in Western Turkey, was assessed. This was achieved by investigating the projected changes and trends of the inflows into the Demirkopru Reservoir, which is the major reservoir in the basin that controls the amount and duration of irrigation water that can be used for the extensive irrigation system in this basin. The analysis in this study involved setting up a coupled hydro-climate model, the WEHY-HCM, over the Gediz Basin by coupling the WRF model (atmospheric component) to the WEHY model (hydrologic component). The WRF model was used to dynamically downscale climatic variables of historical reanalysis and eight future climate projection data into much finer resolutions (6 km) that are more appropriate for watershed hydrologic modeling. Fine temporal and spatial resolution used in this study also enabled the reproducibility of the fine variability patterns of the Mediterranean climate. The downscaled results were then input into the WEHY model to simulate the hydrological processes within the basin, and to obtain the projected future inflows into the Demirkopru Reservoir.

From the analysis of the downscaled climatic variables of the future projections, it was seen that during the early century period (2017–2044), the ensemble average of all eight climate projections showed a significantly increasing trend in basin-scale temperatures, but revealed no expected change in the average annual temperature as compared to the historical values. However, the corresponding values for the mid-century (2045–2072) and the late century (2073–2100) periods revealed an expected increase in the average annual temperature by +1.1 °C and + 2.2 °C, respectively, while showing statistically significant increasing trends for both periods. When the whole 21st century is considered, the average annual temperature of the ensemble of all projections was also projected to increase, this time by +1 °C for all eight projections, with an increasing statistically significant trend as well. Distinguishing between the RCP4.5 and RCP8.5 scenarios revealed that the RCP8.5 scenarios are expected to produce on average a greater increase in basin-scale temperatures (+1.5 °C) as compared to the RCP4.5 scenarios (+0.5 °C). While the ensemble average results of all eight climate projections generally demonstrated increasing trends and a higher expected average annual temperature, there was a significantly large variability among the different projections, which can be attributed mainly to the uncertainty and variability in the GCMs and RCP scenarios.

Such variability was also seen to be translated to the projections of the Demirkopru Reservoir inflows. In fact, both increasing and decreasing trends were found for annual inflows corresponding to different climate projections during the early, mid, and late century periods. Moreover, the expected change in the average annual inflow volumes among different projections as compared to the historical values ranged from −1.9% to +47.0% for the early century, from −9.1% to +83.8% for the mid-century, and from −10.0% to +50.7% for the late century. When considering the ensemble average of all climate projections within these three periods, results showed that the average annual inflow volumes are expected to exceed the historical values by +22.3%, +19.5%, and + 4.1%, for the early, mid-, and late century periods. However, it is clear that these changes become less positive with time throughout the 21st century.

When looking at the projected results of the 21st century as a whole, the average annual inflow volumes into the Demirkopru reservoir for all climate projections are expected to exceed the historical values by amounts ranging from +1.5% for MIROC5 RCP4.5 to 41.4% for CCSM4 RCP4.5. As such, the ensemble of all climate projections also shows an expected increase in the average annual inflow volume of +15.4%, as compared to the historical value. The greater portion of this increase, however, mostly comes from the climate projections using the RCP4.5 scenario, whose ensemble showed a projected increase of +20.7% in the average annual inflow volume, as compared to a + 9.8% increase expected from the projections using the RCP8.5 scenarios. Despite the annual inflows being projected to be higher in the future, these inflows were seen to portray a decreasing trend throughout the 21st century. Such a decreasing trend was significant in five out of the eight climate projections, as well as in the ensemble average of the climate projections using the RCP4.5 scenario, those using the RCP8.5 scenario, and also all of the eight climate projections.

Therefore, while the analyses of this study revealed on average a larger projected reservoir inflow volume per year into the Demirkopru Reservoir during the 21st century as compared to historical value, it is important to consider such results among other factors as well. In fact, it is important to note that the magnitude of the difference between the projected inflow volume and the corresponding historical value decreases throughout the 21st century, when this magnitude becomes the smallest during the late century period, signifying that it will continue to decrease in the following years. Another important factor to consider is that the average annual basin-scale temperature during the 21st century is also projected to exceed the historical value, with trendlines that are consistently, strongly, and significantly increasing throughout the whole 21st century, as well as throughout each of its three periods. As indicated by other climate change impact studies (e.g., Li et al., 2012; Acharjee et al., 2017; Gharbia et al., 2018), increasing temperatures may greatly affect evaporation and transpiration rates which may in turn reduce the amount of water available in the basin. Furthermore, the timings of the reservoir inflows, not just their larger magnitudes, also play an important role both for the operation of the reservoir and for the irrigation system downstream of the reservoir. In this case, a greater inflow volume per year does not automatically translate to a greater irrigation water availability during that year. Therefore, despite the average annual inflow volume during the 21st century being projected to generally exceed the historical value, the opposing roles that the other factors may play could significantly offset the advantages of this projected increase in the average magnitude of the annual inflows. As such, it would be prudent to perform, as a next step, a reservoir simulation and drought analysis in order to determine the effect that such changes may collectively have on the irrigation and water availability inside the Gediz Basin.

Supplementary data to this article can be found online at https://doi.org/10.1016/j.scitotenv.2018.08.167.

References

Acharjee, T.K., Ludwig, F., van Halsema, G., Hellegers, P., Supit, I., 2017. Future changes in water requirements of Boro rice in the face of climate change in North-West Bangladesh. Agric. Water Manag. 194, 172–183. https://doi.org/10.1016/j.agwat.2017.09.008.

Allen, M., Raper, S., Mitchell, J., 2001. Climate change - uncertainty in the IPCC's third assessment report. Science 293 (5529), 430–433. https://doi.org/10.1126/science.1062823.

Amin, M.Z.M., Shaaban, A.J., Ercan, A., Ishida, K., Kavvas, M.L., Chen, Z.Q., Jang, S., 2017. Future climate change impact assessment of watershed scale hydrologic processes in Peninsular Malaysia by a regional climate model coupled with a physically-based hydrology modelo. Sci. Total Environ. 575, 12–22. https://doi.org/10.1016/j.scitotenv.2016.10.009.

Arnell, N.W., 1999a. Climate change and global water resources. Glob. Environ. Chang. 9, S31–S49.

Arnell, N.W., 1999b. The effect of climate change on hydrological regimes in Europe: a continental perspective. Glob. Environ. Chang. 9 (1), 5–23.

Arnell, N.W., 2003. Effects of IPCC SRES emissions scenarios on river runoff: a global perspective. Hydrol. Earth Syst. Sci. 7 (5), 619–641. https://doi.org/10.5194/hess-7-619-2003.

Biricik, A.S., 1995. Gediz Havzasi'nin Su Potansiyeli (Water potential of the Gediz Basin). Turk Cografya Dergisi 30, 13–23 (In Turkish).

Bohner, M.U., Zeman, J., Smiatek, J., Arnold, A., Kastner, J., 2014. Nudged-elastic band used to find reaction coordinates based on the free energy. J. Chem. Phys. 140 (7).

Bolulu, U., 2015. Tüm barajlar doldu Gördes boşaldı (All reservoirs are filled up, except Gordes Dam). Retrieved from. http://www.hurriyet.com.tr/tum-barajlar-doldu-gordes-bosaldi-28777043 (In Turkish).

Cattiaux, J., Douville, H., Peings, Y., 2013. European temperatures in CMIP5: origins of present-day biases and future uncertainties. Clim. Dyn. 41 (11−12), 2889–2907. https://doi.org/10.1007/s00382-013-1731-y.

Chen, J., Brissette, F.P., Leconte, R., 2011. Uncertainty of downscaling method in quantifying the impact of climate change on hydrology. J. Hydrol. 401 (3–4), 190–202. https://doi.org/10.1016/j.jhydrol.2011.02.020.

Christensen, J.H., Christensen, O.B., 2003. Climate modelling: severe summertime flooding in Europe. Nature 421 (6925), 805–806. https://doi.org/10.1038/421805a.

Clarke, L., Edmonds, J., Jacoby, H., Pitcher, H., Reilly, J., Richels, R., 2007. Scenarios of greenhouse gas emissions and atmospheric concentrations. Sub-report 2.1A of Synthesis and Assessment Product 2.1 by the U.S.Climate Change Science Program and the Subcommittee on Global Change Research, Washington, DC., USA

Dee, D.P., Uppala, S.M., Simmons, A.J., Berrisford, P., Poli, P., Kobayashi, S., Andrae, U., Balmaseda, M.A., Balsamo, G., Bauer, P., Bechtold, P., Beljaars, A.C.M., van de Berg, L., Bidlot, J., Bormann, N., Delsol, C., Dragani, R., Fuentes, M., Geer, A.J., Haimberger, L., Healy, S.B., Hersbach, H., Holm, E.V., Isaksen, L., Kallberg, P., Kohler, M., Matricardi, M., McNally, A.P., Monge-Sanz, B.M., Morcrette, J.J., Park, B.K., Peubey, C., de Rosnay, P., Tavolato, C., Thepaut, J.N., Vitart, F., 2011. The ERA-Interim reanalysis: configuration and performance of the data assimilation system. Q. J. R. Meteorol. Soc. 137 (656), 553–597. https://doi.org/10.1002/qj.828.

Droogers, P., Bastiaanssen, W.G.M., Beyazgul, M., Kayam, Y., Kite, G.W., Murray-Rust, H., 2000. Distributed agro-hydrological modeling of an irrigation system in western Turkey. Agric. Water Manag. 43 (2), 183–202. https://doi.org/10.1016/S0378-3774(99)00055-4.

DSI, 2015. Devlet Su Isleri (State Hydraulic Works). Retrieved from. http://www2.dsi.gov.tr/bolge/dsi2/manisa.htm (In Turkish).

Dunne, J.P., John, J.G., Adcroft, A.J., Griffies, S.M., Hallberg, R.W., Shevliakova, E., Stouffer, R.J., Cooke, W., Dunne, K.A., Harrison, M.J., Krasting, J.P., Malyshev, S.L., Milly, P.C.D., Phillipps, P.J., Sentman, L.T., Samuels, B.L., Spelman, M.J., Winton, M., Wittenberg, A.T., Zadeh, N., 2012. GFDL's ESM2 global coupled climate-carbon earth system models. Part I: physical formulation and baseline simulation characteristics. J. Clim. 25 (19), 6646–6665. https://doi.org/10.1175/JCLI-D-11-00560.1.

Dunne, J.P., John, J.G., Shevliakova, E., Stouffer, R.J., Krasting, J.P., Malyshev, S.L., Milly, P.C.D., Sentman, L.T., Adcroft, A.J., Cooke, W., Dunne, K.A., Griffies, S.M., Hallberg, R.W., Harrison, M.J., Levy, H., Wittenberg, A.T., Phillips, P.J., Zadeh, N., 2013. GFDL's ESM2 global coupled climate-carbon earth system models. Part II: carbon system formulation and baseline simulation characteristics. J. Clim. 26 (7), 2247–2267. https://doi.org/10.1175/JCLI-D-12-00150.1.

EEA, 2007. CLC2006 technical guidelines. EEA Technical Report No:17. European Environment Agency, Copenhagen.

EEA, 2017. Climate change, impacts and vulnerability in Europe 2016: an indicator-based report. European Environment Agency Report No: 1/2017 (Luxembourg).

Fowler, H.J., Blenkinsop, S., Tebaldi, C., 2007. Linking climate change modelling to impacts studies: recent advances in downscaling techniques for hydrological modelling. Int. J. Climatol. 27 (12), 1547–1578. https://doi.org/10.1002/joc.1556.

Gent, P.R., Danabasoglu, G., Donner, L.J., Holland, M.M., Hunke, E.C., Jayne, S.R., Lawrence, D.M., Neale, R.B., Rasch, P.J., Vertenstein, M., Worley, P.H., Yang, Z.L., Zhang, M.H., 2011. The community climate system model version 4. J. Clim. 24 (19), 4973–4991. https://doi.org/10.1175/2011JCLI4083.1.

Gerten, D., Rost, S., von Bloh, W., Lucht, W., 2008. Causes of change in 20th century global river discharge. Geophys. Res. Lett. 35 (20). https://doi.org/10.1029/2008GL035258.

Gharbia, S.S., Smullen, T., Gill, L., Johnston, P., Pilla, F., 2018. Spatially distributed potential evapotranspiration modeling and climate projections. Sci. Total Environ. 633, 571–592. https://doi.org/10.1016/j.scitotenv.2018.03.208.

Giorgi, F., Francisco, R., 2000. Uncertainties in regional climate change prediction: a regional analysis of ensemble simulations with the HADCM2 coupled AOGCM. Clim. Dyn. 16 (2–3), 169–182.

Gleick, P.H., 1989. Climate change, hydrology, and water-resources. Rev. Geophys. 27 (3), 329–344.

Graham, L.P., Hagemann, S., Jaun, S., Beniston, M., 2007. On interpreting hydrological change from regional climate models. Clim. Chang. 81, 97–122. https://doi.org/10.1007/s10584-006-9217-0.

Hakyemez, H.Y., Goktas, F., Erkal, T., 2013. Quaternary geology and evolution of the Gediz graben. Geol. Bull. Turk. 56 (2), 1–26.

HEC-GeoHMS, 2013. Geospatial Hydrologic Modeling Extension User's Manual. (CPD-77). US Army Corps of Engineers, Hydrologic Engineering Center.

Hertig, E., Jacobeit, J., 2008. Downscaling future climate change: temperature scenarios for the Mediterranean area. Glob. Planet. Chang. 63 (2–3), 127–131. https://doi.org/10.1016/j.gloplacha.2007.09.003.

Hidalgo, H.G., Das, T., Dettinger, M.D., Cayan, D.R., Pierce, D.W., Barnett, T.P., Bala, G., Mirin, A., Wood, A.W., Bonfils, C., Santer, B.D., Nozawa, T., 2009. Detection and attribution of streamflow timing changes to climate change in the western United States. J. Clim. 22 (13), 3838–3855. https://doi.org/10.1175/2009JCLI2470.1.

Hong, S.Y., Dudhia, J., Chen, S.H., 2004. A revised approach to ice microphysical processes for the bulk parameterization of clouds and precipitation. Mon. Weather Rev. 132 (1), 103–120. https://doi.org/10.1175/1520-0493(2004)132<0103:ARATIM>2.0.CO;2.

Hong, S.Y., Noh, Y., Dudhia, J., 2006. A new vertical diffusion package with an explicit treatment of entrainment processes. Mon. Weather Rev. 134 (9), 2318–2341. https://doi.org/10.1175/MWR3199.1.

IPCC, 2014. Climate change 2014: synthesis report. In: Team, C.W., Pachauri, R.K., Meyer, L.A. (Eds.), Contribution of Working Groups I, II and III to the Fifth Assessment Report of the Intergovernmental Panel on Climate Change. IPCC, Geneva, Switzerland, p. 151.

Ishida, K., Gorguner, M., Ercan, A., Trinh, T., Kavvas, M.L., 2017. Trend analysis of watershed-scale precipitation over Northern California by means of dynamically-downscaled CMIP5 future climate projections. Sci. Total Environ. 592, 12–24. https://doi.org/10.1016/j.scitotenv.2017.03.086.

ISRIC, 2013. World soil information. SoilGrids: An Automated System for Global Soil Mapping.

Jang, S., Kavvas, M.L., 2015. Downscaling global climate simulations to regional scales: statistical downscaling versus dynamical downscaling. J. Hydrol. Eng. 20 (1). https://doi.org/10.1061/(ASCE)HE.1943-5584.0000939.

Jang, S., Kavvas, M.L., Ishida, K., Trinh, T., Ohara, N., Kure, S., Chen, Z.Q., Anderson, M.L., Matanga, G., Carr, K.J., 2017. A performance evaluation of dynamical downscaling of precipitation over Northern California. Sustainability 9 (8). https://doi.org/10.3390/su9081457.

Jones, C.D., Hughes, J.K., Bellouin, N., Hardiman, S.C., Jones, G.S., Knight, J., Liddicoat, S., O'Connor, F.M., Andres, R.J., Bell, C., Boo, K.O., Bozzo, A., Butchart, N., Cadule, P., Corbin, K.D., Doutriaux-Boucher, M., Friedlingstein, P., Gornall, J., Gray, L., Halloran, P.R., Hurtt, G., Ingram, W.J., Lamarque, J.F., Law, R.M., Meinshausen, M., Osprey, S., Palin, E.J., Chini, L.P., Raddatz, T., Sanderson, M.G., Sellar, A.A., Schurer, A., Valdes, P., Wood, N., Woodward, S., Yoshioka, M., Zerroukat, M., 2011. The HadGEM2-ES implementation of CMIP5 centennial simulations. Geosci. Model Dev. 4 (3), 543–570. https://doi.org/10.5194/gmd-4-543-2011.

Kavvas, M.L., Chen, Z.Q., Tan, L., Soong, S.T., Terakawa, A., Yoshitani, J., Fukami, K., 1998. A regional-scale land surface parameterization based on areally-averaged hydrological conservation equations. Hydrol. Sci. J. 43 (4), 611–631. https://doi.org/10.1080/02626669809492157.

Kavvas, M.L., Chen, Z.Q., Dogrul, C., Yoon, J.Y., Ohara, N., Liang, L., Aksoy, H., Anderson, M.L., Yoshitani, J., Fukami, K., Matsuura, T., 2004. Watershed Environmental Hydrology (WEHY) model based on upscaled conservation equations: hydrologic module. J. Hydrol. Eng. 9 (6), 450–464. https://doi.org/10.1061/(ASCE)1084-0699(2004)9:6(450).

Kavvas, M.L., Kure, S., Chen, Z.Q., Ohara, N., Jang, S., 2013. WEHY-HCM for modeling interactive atmospheric-hydrologic processes at watershed scale. I: model description. J. Hydrol. Eng. 18 (10), 1262–1271. https://doi.org/10.1061/(ASCE)HE.1943-5584.0000724.

Kelley, C., Ting, M.F., Seager, R., Kushnir, Y., 2012. Mediterranean precipitation climatology, seasonal cycle, and trend as simulated by CMIP5. Geophys. Res. Lett. 39. https://doi.org/10.7916/D8CJ8Q5X.

Koralay, O.E., 2015. Late Neoproterozoic granulite facies metamorphism in the Menderes Massif, Western Anatolia/Turkey: implication for the assembly of Gondwana. Geodin. Acta 27 (4), 244–266. https://doi.org/10.1080/09853111.2015.1014987.

Kundzewicz, Z.W., Mata, L.J., Arnell, N.W., Doll, P., Jimenez, B., Miller, K., Oki, T., Sen, Z., Shiklomanov, I., 2008. The implications of projected climate change for freshwater resources and their management. Hydrol. Sci. J. 53 (1), 3–10.

Kure, S., Jang, S., Ohara, N., Kavvas, M.L., Chen, Z.Q., 2013. WEHY-HCM for modeling interactive atmospheric-hydrologic processes at watershed scale. II: model application to ungauged and sparsely gauged watersheds. J. Hydrol. Eng. 18 (10), 1272–1281. https://doi.org/10.1061/(ASCE)HE.1943-5584.0000701.

Lehner, B., Doll, P., Alcamo, J., Henrichs, T., Kaspar, F., 2006. Estimating the impact of global change on flood and drought risks in Europe: a continental, integrated analysis. Clim. Chang. 75 (3), 273–299. https://doi.org/10.1007/s10584-006-6338-4.

Li, Z., Zheng, F.L., Liu, W.Z., 2012. Spatiotemporal characteristics of reference evapotranspiration during 1961–2009 and its projected changes during 2011–2099 on the Loess Plateau of China. Agric. For. Meteorol. 154, 147–155. https://doi.org/10.1016/j.agrformet.2011.10.019.

Li, F.P., Zhang, Y.Q., Xu, Z.X., Teng, J., Liu, C.M., Liu, W.F., Mpelasoka, F., 2013. The impact of climate change on runoff in the southeastern Tibetan Plateau. J. Hydrol. 505, 188–201. https://doi.org/10.1016/j.jhydrol.2013.09.052.

Maraun, D., Wetterhall, F., Ireson, A.M., Chandler, R.E., Kendon, E.J., Widmann, M., Brienen, S., Rust, H.W., Sauter, T., Themessl, M., Venema, V.K.C., Chun, K.P., Goodess, C.M., Jones, R.G., Onof, C., Vrac, M., Thiele-Eich, I., 2010. Precipitation downscaling under climate change: recent developments to bridge the gap between dynamical models and the end user. Rev. Geophys. 48. https://doi.org/10.1029/2009RG000314.

Mccuen, R.H., Rawls, W.J., Brakensiek, D.L., 1981. Statistical-analysis of the Brooks-Corey and the Green-Ampt parameters across soil textures. Water Resour. Res. 17 (4), 1005–1013.
McGuffie, K., Henderson-Sellers, A., 2001. Forty years of numerical climate modelling. Int. J. Climatol. 21 (9), 1067–1109. https://doi.org/10.1002/joc.632.
Moss, R.H., Edmonds, J.A., Hibbard, K.A., Manning, M.R., Rose, S.K., van Vuuren, D.P., Carter, T.R., Emori, S., Kainuma, M., Kram, T., Meehl, G.A., Mitchell, J.F.B., Nakicenovic, N., Riahi, K., Smith, S.J., Stouffer, R.J., Thomson, A.M., Weyant, J.P., Wilbanks, T.J., 2010. The next generation of scenarios for climate change research and assessment. Nature 463 (7282), 747–756. https://doi.org/10.1038/nature08823.
New, M., Hulme, M., 2000. Representing uncertainty in climate change scenarios: a Monte-Carlo approach. Integr. Assess. 1 (3), 203–213. https://doi.org/10.1023/A:1019144202120.
Nohara, D., Kitoh, A., Hosaka, M., Oki, T., 2006. Impact of climate change on river discharge projected by multimodel ensemble. J. Hydrometeorol. 7 (5), 1076–1089. https://doi.org/10.1175/JHM531.1.
Ohara, N., Kavvas, M.L., 2006. Field observations and numerical model experiments for the snowmelt process at a field site. Adv. Water Resour. 29 (2), 194–211. https://doi.org/10.1016/j.advwatres.2005.03.016.
Ohara, N., Kavvas, M.L., Chen, Z.Q., 2008. Stochastic upscaling for snow accumulation and melt processes with PDF approach. J. Hydrol. Eng. 13 (12), 1103–1118. https://doi.org/10.1061/(ASCE)1084-0699(2008)13:12(1103).
Ohara, N., Chen, Z.Q., Kavvas, M.L., Fukami, K., Inomata, H., 2011. Reconstruction of historical atmospheric data by a hydroclimate model for the Mekong River basin. J. Hydrol. Eng. 16 (12), 1030–1039. https://doi.org/10.1061/(ASCE)HE.1943-5584.0000168.
Piao, S.L., Friedlingstein, P., Ciais, P., de Noblet-Ducoudre, N., Labat, D., Zaehle, S., 2007. Changes in climate and land use have a larger direct impact than rising CO2 on global river runoff trends. Proc. Natl. Acad. Sci. U. S. A. 104 (39), 15242–15247. https://doi.org/10.1073/pnas.0707213104.
Praskievicz, S., Chang, H.J., 2009. A review of hydrological modelling of basin-scale climate change and urban development impacts. Prog. Phys. Geogr. 33 (5), 650–671. https://doi.org/10.1177/0309133309348098.
Raisanen, J., Palmer, T.N., 2001. A probability and decision-model analysis of a multimodel ensemble of climate change simulations. J. Clim. 14 (15), 3212–3226. https://doi.org/10.1175/1520-0442(2001)014<3212:APADMA>2.0.CO;2.
Rawls, W.J., Brakensiek, D.L., Saxton, K.E., 1982. Estimation of soil-water properties. Trans. ASABE 25 (5), 1316–1320.
Riahi, K., Rao, S., Krey, V., Cho, C.H., Chirkov, V., Fischer, G., Kindermann, G., Nakicenovic, N., Rafaj, P., 2011. RCP 8.5-a scenario of comparatively high greenhouse gas emissions. Clim. Chang. 109 (1–2), 33–57. https://doi.org/10.1007/s10584-011-0149-y.
Schulze, R.E., 1997. Impacts of global climate change in a hydrologically vulnerable region: challenges to South African hydrologists. Prog. Phys. Geogr. 21 (1), 113–136.
Sen, B., 2015. Gördes kurudu (Gördes dried). Retrieved from. http://www.hurriyet.com.tr/gordes-kurudu-29771042 (In Turkish).
Sillmann, J., Kharin, V.V., Zwiers, F.W., Zhang, X., Bronaugh, D., 2013. Climate extremes indices in the CMIP5 multimodel ensemble: part 2. Future climate projections. J. Geophys. Res.-Atmos. 118 (6), 2473–2493. https://doi.org/10.1002/jgrd.50188.
Skamarock, W.C., Klemp, J.B., Dudhia, J., Gill, D.O., Barker, M., Duda, K.G., Huang, Y., Wang, W., Powers, J.G., 2008. A description of the advanced research WRF version 3. NCAR Technical Note NCAR/TN-475+STR. NCAR, Boulder, Colorado, USA.
Smiatek, G., Kunstmann, H., Heckl, A., 2014. High-resolution climate change impact analysis on expected future water availability in the Upper Jordan catchment and the Middle East. J. Hydrometeorol. 15 (4), 1517–1531. https://doi.org/10.1175/JHM-D-13-0153.1.
Smirnova, T.G., Brown, J.M., Benjamin, S.G., 1997. Performance of different soil model configurations in simulating ground surface temperature and surface fluxes. Mon. Weather Rev. 125 (8), 1870–1884. https://doi.org/10.1175/1520-0493(1997)125<1870:PODSMC>2.0.CO;2.
Smirnova, T.G., Brown, J.M., Benjamin, S.G., Kim, D., 2000. Parameterization of cold-season processes in the MAPS land-surface scheme. J. Geophys. Res.-Atmos. 105 (D3), 4077–4086. https://doi.org/10.1029/1999JD901047.
Smith, S.J., Wigley, T.M.L., 2006. Multi-gas forcing stabilization with Minicam. Energy J. 373–391.
Spak, S., Holloway, T., Lynn, B., Goldberg, R., 2007. A comparison of statistical and dynamical downscaling for surface temperature in North America. J. Geophys. Res.-Atmos. 112 (D8). https://doi.org/10.1029/2005JD006712.
Svendsen, M., Murray-Rust, D.H., Harmancioglu, N., Alpaslan, N., 2005. Governing closing basins: the case of the Gediz River in Turkey. In: Svendsen, M. (Ed.), Irrigation and River Basin Management: Options for Governance and Institutions. CABI Publishing, Colombo, Sri Lanka.
Taylor, K.E., Stouffer, R.J., Meehl, G.A., 2012. An overview of CMIP5 and the experiment design. Bull. Am. Meteorol. Soc. 93 (4), 485–498. https://doi.org/10.1175/BAMS-D-11-00094.1.
Tebaldi, C., Knutti, R., 2007. The use of the multi-model ensemble in probabilistic climate projections. Philos. Trans. R. Soc. A Math. Phys. Eng. Sci. 365 (1857), 2053–2075. https://doi.org/10.1098/rsta.2007.2076.
Tiedtke, M., 1989. A comprehensive mass flux scheme for cumulus parameterization in large-scale models. Mon. Weather Rev. 117 (8), 1779–1800. https://doi.org/10.1175/1520-0493(1989)117<1779:ACMFSF>2.0.CO;2.
Trzaska, S., Schnarr, E., 2014. A Review of Downscaling Methods for Climate Change Projections: African and Latin American Resilience to Climate Change (ARCC) Project.
Turkes, M., 1996. Spatial and temporal analysis of annual rainfall variations in Turkey. Int. J. Climatol. 16 (9), 1057–1076. https://doi.org/10.1002/(SICI)1097-0088(199609)16:9<1057::AID-JOC75>3.0.CO;2-D.
ul Hasson, S., Pascale, S., Lucarini, V., Bohner, J., 2016. Seasonal cycle of precipitation over major river basins in South and Southeast Asia: a review of the CMIP5 climate models data for present climate and future climate projections. Atmos. Res. 180, 42–63. https://doi.org/10.1016/j.atmosres.2016.05.008.
Ulke, A., Tayfur, G., Ozkul, S., 2009. Predicting suspended sediment loads and missing data for Gediz River, Turkey. J. Hydrol. Eng. 14 (9), 954–965. https://doi.org/10.1061/(ASCE)HE.1943-5584.0000060.
van Vliet, M.T.H., Franssen, W.H.P., Yearsley, J.R., Ludwig, F., Haddeland, I., Lettenmaier, D.P., Kabat, P., 2013. Global river discharge and water temperature under climate change. Glob. Environ. Chang. 23 (2), 450–464. https://doi.org/10.1016/j.gloenvcha.2012.11.002.
van Vuuren, D.P., Edmonds, J., Kainuma, M., Riahi, K., Thomson, A., Hibbard, K., Hurtt, G.C., Kram, T., Krey, V., Lamarque, J.F., Masui, T., Meinshausen, M., Nakicenovic, N., Smith, S.J., Rose, S.K., 2011. The representative concentration pathways: an overview. Clim. Chang. 109 (1–2), 5–31. https://doi.org/10.1007/s10584-011-0148-z.
Watanabe, M., Suzuki, T., O'ishi, R., Komuro, Y., Watanabe, S., Emori, S., Takemura, T., Chikira, M., Ogura, T., Sekiguchi, M., Takata, K., Yamazaki, D., Yokohata, T., Nozawa, T., Hasumi, H., Tatebe, H., Kimoto, M., 2010. Improved climate simulation by MIROC5: mean states, variability, and climate sensitivity. J. Clim. 23 (23), 6312–6335. https://doi.org/10.1175/2010JCLI3679.1.
Webster, M., Forest, C., Reilly, J., Babiker, M., Kicklighter, D., Mayer, M., Prinn, R., Sarofim, M., Sokolov, A., Stone, P., Wang, C., 2003. Uncertainty analysis of climate change and policy response. Clim. Chang. 61 (3), 295–320.
Wilby, R.L., Harris, I., 2006. A framework for assessing uncertainties in climate change impacts: low-flow scenarios for the River Thames, UK. Water Resour. Res. 42 (2). https://doi.org/10.1029/2005WR004065.
Wilby, R.L., Wigley, T.M.L., 1997. Downscaling general circulation model output: a review of methods and limitations. Prog. Phys. Geogr. 21 (4), 530–548.
Wilby, R.L., Wigley, T.M.L., Conway, D., Jones, P.D., Hewitson, B.C., Main, J., Wilks, D.S., 1998. Statistical downscaling of general circulation model output: a comparison of methods. Water Resour. Res. 34 (11), 2995–3008. https://doi.org/10.1029/98WR02577.
Wilby, R.L., Whitehead, P.G., Wade, A.J., Butterfield, D., Davis, R.J., Watts, G., 2006. Integrated modelling of climate change impacts on water resources and quality in a lowland catchment: River Kennet, UK. J. Hydrol. 330 (1–2), 204–220. https://doi.org/10.1016/j.jhydrol.2006.04.033.
Wise, M., Calvin, K., Thomson, A., Clarke, L., Bond-Lamberty, B., Sands, R., Smith, S.J., Janetos, A., Edmonds, J., 2009. Implications of limiting CO2 concentrations for land use and energy. Science 324 (5931), 1183–1186. https://doi.org/10.1126/science.1168475.
WRF-ARW, 2015. WRF-ARW Version 3 Modeling System User's Guide.
Xu, C.Y., 1999. From GCMs to river flow: a review of downscaling methods and hydrologic modelling approaches. Prog. Phys. Geogr. 23 (2), 229–249.
Yilmaz, B., Harmancioglu, N.B., 2010. An indicator based assessment for water resources management in Gediz River Basin, Turkey. Water Resour. Manag. 24 (15), 4359–4379. https://doi.org/10.1007/s11269-010-9663-3.
Yilmaz, B., Harmancioglu, N.B., 2012. Comparative assessment of water management indicators in the Gediz river basin with foreseen climate scenarios. J. Eur. Water 37, 27–32.
Zanis, P., Katragkou, E., Ntogras, C., Marougianni, G., Tsikerdekis, A., Feidas, H., Anadranistakis, E., Melas, D., 2015. Transient high-resolution regional climate simulation for Greece over the period 1960–2100: evaluation and future projections. Clim. Res. 64 (2), 123–140. https://doi.org/10.3354/cr01304.
Zhang, C., Wang, Y., Hamilton, K., 2011. Improved representation of boundary layer clouds over the Southeast Pacific in ARW-WRF using a modified Tiedtke cumulus parameterization scheme. Mon. Weather Rev. 139 (11), 3489–3513. https://doi.org/10.1175/MWR-D-10-05091.1.